Physics – Uspekhi **57** (8) 771 – 786 (2014)

REVIEWS OF TOPICAL PROBLEMS PACS numbers: 05.70.Fh, 05.70.Ln, **68.70.+w**

Dendrite growth under forced convection: analysis methods and experimental tests

D V Alexandrov, P K Galenko

DOI: 10.3367/UFNe.0184.201408b.0833

Contents

Abstract. An analysis is given of the nonisothermal growth of a dendrite crystal under forced fluid flow in a binary system. The theoretical model utilized employs a free moving crystal–liquid interface and makes use of the Oseen approximation for the equations of motion of the liquid. A criterion for the stable growth of two-dimensional and three-dimensional parabolic dendrites is derived under the assumption of an anisotropic surface tension at the crystal–liquid interface, which generalizes the previous known results for the stable growth of a dendrite with convection in a one-component fluid and for the growth of a dendrite in a two-component system at rest. The criterion obtained within the Oseen hydrodynamic approximation is extended to arbitrary Peclet numbers and dendrite growth with convection in a nonisothermal multicomponent system. Model predictions are compared with experimental data on crystal growth kinetics in droplets processed in electromagnetic and electrostatic levitation facilities. Theoretical and simulation methods currently being developed are applied to crystallization processes under earthly and reduced gravity conditions.

D V Alexandrov. Department of Mathematical Physics,
Ural Federal University,
prosp. Lenina 51, 620083 Ekaterinburg, Russian Federation
E-mail: dmitri.alexandrov@urfu.ru
P K Galenko. Friedrich-Schiller-Universität-Jena,
Physikalisch-Astronomische Fakultät,
Löbdergraben Strasse 32, 07743 Jena, Germany;
Institut für Materialphysik im Weltraum,
Deutsches Zentrum für Luft- und Raumfahrt (DLR),
51170 Köln, Germany
E-mail: peter.galenko@uni-jena.de

Received 17 December 2013, revised 18 March 2014
Uspekhi Fizicheskikh Nauk **184** (8) 833 – 850 (2014)
DOI: 10.3367/UFNr.0184.201408b.0833
Translated by Yu V Morozov; edited by A Radzig

1. Introduction

Dendrites are ramified treelike crystals composed of a trunk and groups of branches oriented along the main crystallographic axes of the lattice [1–6]. The dendritic shape represents the most common morphological form of crystals emerging from supercooled melts and supersaturated solutions. The mass and heat transfer processes and kinetics of atomic attachment at the interface control both the growth rate and the dispersiveness of the dendritic structure that eventually forms on mesoscopic and macroscopic spatial length scales ($\sim 10^{-6}-10^{-3}$ m) [7–9]. Figure 1 shows the well-developed surface of a dendritic crystal grown in a supercooled melt.

Theoretical analysis and computer simulation implicated in the investigation of dendritic morphology are as important as observations of crystal growth dynamics [11–13]. Qualitatively new data obtained in recent years can be utilized to verify the major concepts of dendritic crystal formation [14]. Of special interest in this context are two problems having important theoretical and practical implications: the stability of free space dendritic tip growth, and the influence of convective flow on the mechanism of growth regime selection [15–17].

The former problem arose from the analysis of the Ivantsov model [18–20] and experimental data on the growth of the needle crystal with a paraboloidal tip [21–27]. The analysis led to the conclusion that the continuous family of Ivantsov's isotropic solutions is unstable, i.e., the paraboloi-

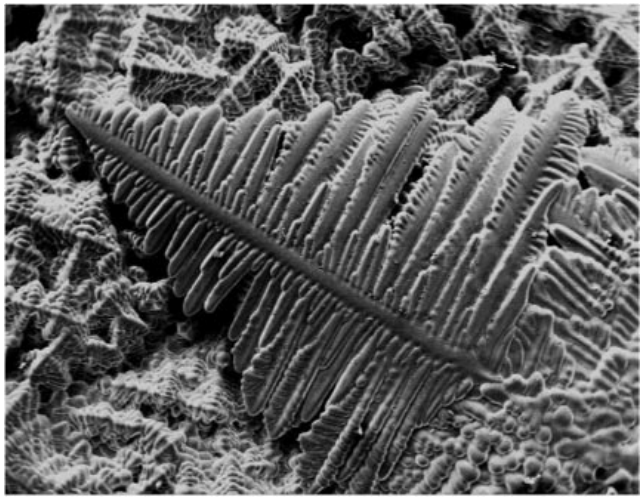

Figure 1. Dendritic crystal in the cross section through a solidified metallic melt treated in an electromagnetic levitator (electron micrograph) [10]. The dendrite central trunk is 100 μm long.

dal shape of a needle crystal is unstable in the steady-state growth regime [28, 29]. It was shown that the crystalline anisotropy of the physical properties of the mobile crystal–liquid interface stabilizes the dendrite paraboloidal shape. Therefore, the Ivantsov solution was taken as a zero approximation in the search for a solution to stable growth in the first approximation in which the role of the small parameter is played by the anisotropy of surface tension or growth kinetics [29].

Following establishment of the criterion for dendritic tip stability in a stagnant one-component medium [28, 29], the problem was extended to convective medium motion [30–32] and dendritic crystal growth in a binary (chemically two-component) medium without convection [33]. In many real situations, however, a comparative analysis of dendrite growth in a binary system has to take into consideration convective flows [34]. Moreover, nonisothermal solidification of binary melts is, as a rule, accompanied by the chemical segregation in the solid phase being formed, leading to the production of inhomogeneous solid solutions and disordered crystal structures and the development of crystal heterogranularity. Evidently, this accounts for the marked variability of the physical, mechanical, electric, and chemical properties of the samples and materials thus obtained [9, 35–37].

The present review is concerned with the comprehensive consideration of the selection of the stable dendritic tip growth regime in a binary system under forced convective flow of the liquid phase.

Natural convection (e.g., thermogravitational or thermocapillary convection under terrestrial and microgravity conditions, respectively) and forced convective flow of liquid play a key role in transfer processes at the crystal–melt interface. Convective flows significantly change local gradients of temperature and impurity concentration; thereby, they affect evolutionary patterns of the solidification front [38]. In the special case of dendritic structures, their shape and growth rate are governed by temperature and concentration gradients established as a result of both the conductive (molecular) and convective heat and mass transfer near the moving interface [38–40]. Both experiment and simple estimating calculations [39, 40], as well as the phase field

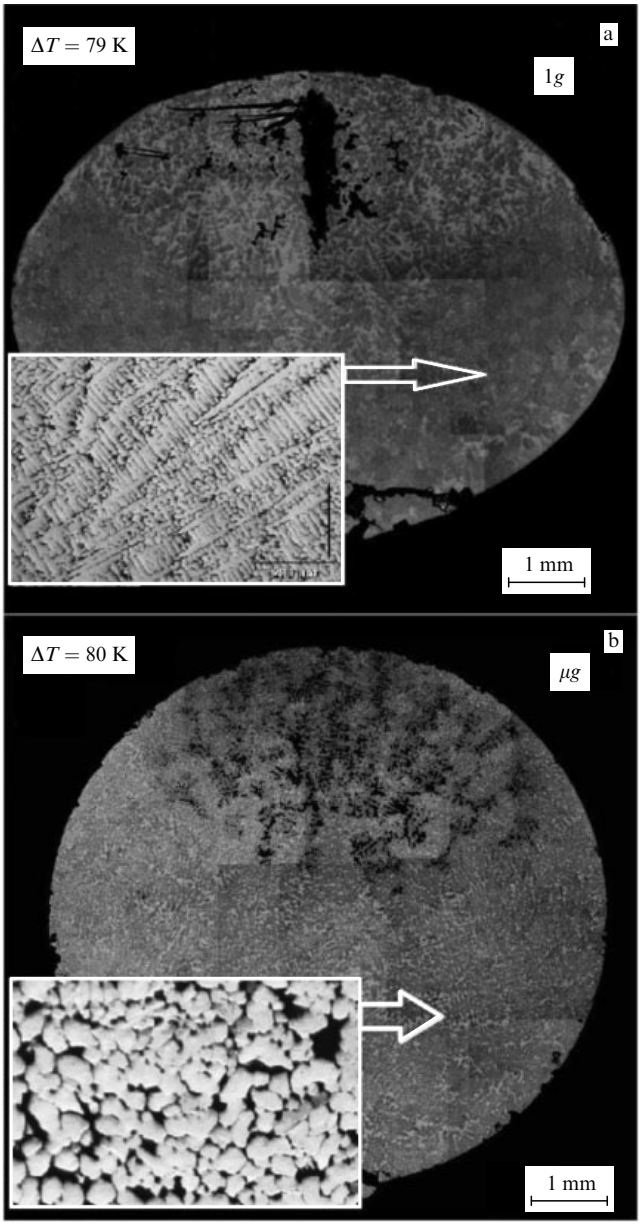

Figure 2. Microstructure of an Ni_{60}-Al_{40} alloy droplet [48] crystallized under terrestrial (1g) (a) and microgravity (b) conditions. The insets images magnified fragments of the microstructure.

modeling [41–43], have demonstrated the strong influence of melt convection on the formation of a dendritic structure growing into a supercooled liquid flow. Convection was shown to affect phase selection [44–46], grain refinement [34, 47], and crystal structure formation [48, 49].

Figure 2 compares microstructures of Ni-Al alloy samples crystallized under terrestrial conditions at normal gravity (1g) and under microgravity conditions. Forced convection induced under terrestrial conditions by an alternating electromagnetic field caused formation of extended and unbroken dendritic crystals (Fig. 2a). Crystallization in a stagnant melt results in a solidified microstructure in the form of fragmented dendritic crystals (Fig. 2b). Due to the absence of convective heat transport during solidification under microgravity, a droplet remains in the two-phase state longer than under 1g conditions. It produces the grain-refinement effect [50, 51], and the final microstructure turns out to be much

denser for samples crystallized under microgravity conditions.

A dendrite growth model extending an earlier theory [52, 53] was proposed in Ref. [16]. This model describes the dependence of the dendrite growth rate on supercooling in the incident convective fluid flow. In stating the problem, the authors made use of the hydrodynamic equations for an ideal fluid with zero viscosity, which substantially simplifies the theoretical description of fluids. Later on, this theory was advanced to describe the dendrite growth in the event of real fluids possessing the property of viscosity [54, 55].

The objective of the present review consists in considering recent experimental data, results of numerical simulations, and theoretical analyses of the influence of forced fluid flows on the characteristics of dendritic crystal growth. The model description leans upon analytical results from Ref. [55] giving a solution to the problem of nonisothermal dendrite growth in a binary melt in the presence of counter flow of fluid. Such a model description is needed for the quantitative assessment and prediction of the properties of samples made from specially purified materials and alloy systems undergoing containerless processing under terrestrial and reduced gravity conditions [56]. The problem statement is in accordance with the Stefan model including the anisotropy of the surface energy at the parabolic (and paraboloidal) crystal–liquid interface. The problem for the forced flow is solved in the Oseen approximation due to the smallness of the Reynolds number. An analysis of the stable regime in the framework of such a generalized model yields a criterion for dendritic tip growth in a binary system with convection, making it possible to predict crystal growth kinetics by correlation with experimental measurements of crystal growth rate and morphological characteristics depending on convective flow intensity.

2. Convective flow in droplets solidified in levitators

Containerless and crucibless techniques, such as the drop tube method, atomization, and levitation, substantially decrease the probability of the heterogeneous nucleation of stable centers of a new phase on the surface of a sample being processed. As a result, samples can be supercooled hundreds of degrees in the course of slow (e.g., in levitators) or intense (as in fast quenching from the liquid phase) cooling. The temperature of the sample may decrease in the process at a rate of several million degrees per second, e.g., during atomization, under high-intensity laser recrystallization, in drop tubes, or in splat quenching [57]. Both slow and intense cooling bring the sample to a metastable state, and the formation of its structure is mediated through the formation of metastable intermediate and long-lived phases [9].

The morphological and dynamic features of crystal growth were actively studied by direct observation of crystallization of optically transparent samples [38, 58–60]. Experiments with optically nontransparent droplets were carried out by acoustic, electrostatic, and electromagnetic levitation techniques as unique methods for supercooling metallic and alloy samples with a diameter from a few micrometers to 1 cm. These methods are equally efficacious for controlled crystal nucleation initiated from the outside and the observation of crystallization front propagation. Levitation techniques for containerless processing of shots and drops are overviewed in Refs [9, 36, 61].

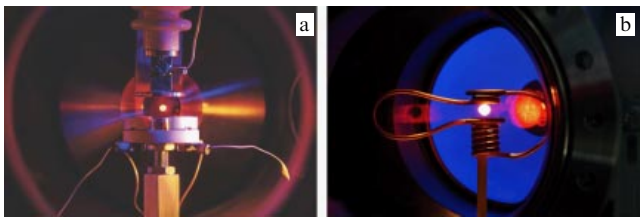

Figure 3. Overall view of levitation facilities with samples. (a) Levitation of a liquid sample (droplet) in an electrostatic levitator in an ultrahigh vacuum. (b) Levitation of a droplet in an electromagnetic levitator with the application of an alternating electromagnetic field.

Figure 3 shows electrostatic levitator (ESL) and electromagnetic levitator (EML) facilities employed in experiments on heating and cooling shots with the initiation of crystallization under controlled supercooling conditions or spontaneous avalanche high-speed solidification. In ESL (Fig. 3a), a sample levitates under the effect of the electrostatic force arose between two disks. Technical details pertaining to ESL are described, e.g., in paper [62]. In EML (Fig. 3b), a sample levitates in a nonuniform electromagnetic field generated by a conical (sometimes cylindrical) coil.

The preliminary cyclic 'heating–cooling' treatment is effected by the containerless (crucibless) technique, in which the walls (volume, shape) of the container do not exert influence on heterogeneous nucleation of a new phase. This approach allows strong supercooling (several hundred degrees) to be reached in the liquid phase of the sample. As a result, it solidifies at a high rate of up to 100 m s^{-1}. The rapid crystallization front is recorded by a videocamera with a writing speed of up to 4×10^5 frames per second.

In the case of sample levitation in ESL, forced convection is absent due to an electrostatic field [62–65]. However, an ESL experiment is long enough for Marangoni (thermocapillary) convection, at which the maximum flow rate reaches a few centimeters per second: $U \lesssim 0.05$ m s^{-1}. This value lies at the limit of accuracy of the method for measuring the crystal growth rate in ESL. For this reason, it is usually assumed in terrestrial ESL experiments that Marangoni's convective flow can influence crystal growth only under small or vanishingly small supercooling. In contrast, melting a shot in EML and its further cyclic processing are associated with intense forced convection in the drop liquid phase [62–65, 67] that may have a marked effect on crystal morphology and growth kinetics.

Figure 4 shows schematically the central part of the EML facility with a levitating droplet. When alternating current passes through the coil, the electromagnetic field induces eddy currents in the hard electrically conductive shot. These currents give rise to a repulsive force (Lorentz force $\mathbf{F}_L$) directed opposite to both the main field and the heat release (the cause of shot melting). As gravitational and Lorentz forces become equal, i.e., at $|\mathbf{F}_L| = |\mathbf{F}_g|$, the shot begins to levitate and simultaneously melt when heated. Then, the melted shot in the form of a liquid droplet can be supercooled to a temperature below the equilibrium solidification temperature by a cooling gas that passes through the working volume of EML. Solidification can either be initiated by a trigger needle made of the same material as the starting shot or occur spontaneously The release of latent heat accounts for heating the crystallizible part of the sample with a recalescence front that is the geometric envelope of primary crystal tips

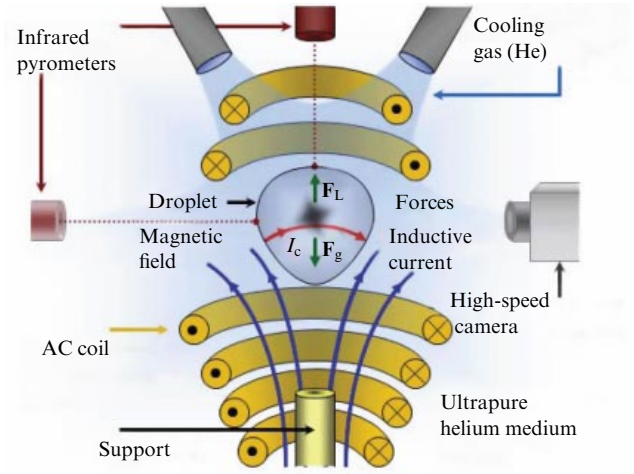

Figure 4. Levitating sample (droplet, shot) in the coil of an electromagnetic levitator (the schematic taken from Ref. [66]). The sample levitates due to the equality between gravity force $\mathbf{F}_g$ and Lorentz force $\mathbf{F}_L$, i.e., at $|\mathbf{F}_L| = |\mathbf{F}_g|$; I_c is the current induced in the droplet by an alternating electromagnetic field.

usually having a dendritic structure. Heat and mass transfers in the recalescence front control the growth dynamics of such dendritic crystals. Computed images obtained with a high-speed video camera make it possible to record the recalescence front and quantitatively evaluate its propagation velocity in the supercooled droplet [9, 17, 67].

The alternating magnetic field induces an electric current that causes the melt to move so that the flow inside the droplet splits into two. As shown in Fig. 5, two spatial tori are formed in the fluid structure: the flow in the center of the sample (at the bottom of the droplet, near its southern pole) is directed downward, while at the top (near the northern pole) it is directed upward. Soon after the onset of droplet solidification, a convective flow with the mean velocity U is directed towards the growing dendrites in the lower part of the droplet,

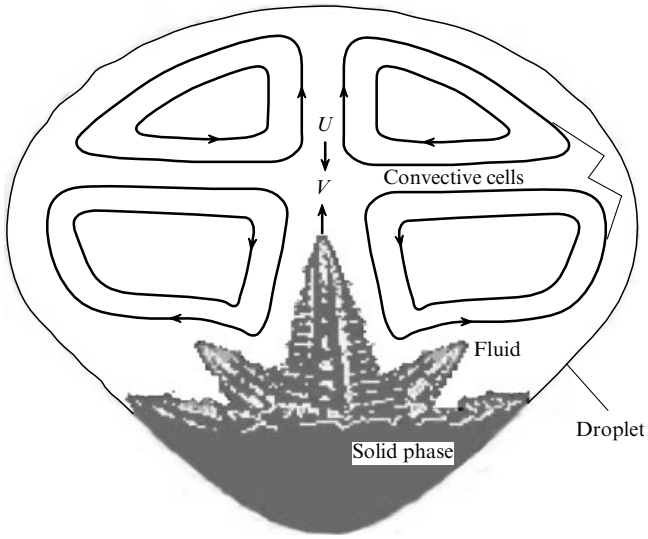

Figure 5. Schematic of current lines in convective cells of the liquid phase during dendritic crystallization of a droplet in an electromagnetic levitator [17]. Two-dimensional cross section through the droplet shows the cellular structure of the liquid represented in three dimensions by two tori; V — dendritic tip growth rate, and U — averaged fluid flow velocity.

resulting in a rise in growth rate V and the formation of mostly developed main dendritic trunks growing towards the flow of the liquid phase (see Fig. 5). The results of calculations of convective structures in the droplets processed in EML [63, 64, 68] confirm the hypothetical scheme of convective tori formed during crystallization [16, 17]. The governing equations of the model can be formulated based on the scheme depicted in Fig. 5.

3. Crystal growth model

Crystal growth in the incoming flow of fluid is described in terms of the nonlinear Stefan type thermodiffusion problem [69, 70] with the moving free boundary of phase transition. Temperature $T_{\rm int}$ of the crystal–liquid interface depends on its local curvature $1/R$, crystallization temperature T_0 of pure matter, surface tension coefficient σ, and latent crystallization heat Q:

$$T_{\rm int} = T_0 - \frac{T_0\sigma}{QR}\,. \tag{1}$$

Temperatures of solid (T_s) and liquid (T_l) phases taking account of the incoming flow of fluid are given by the heat conduction equation

$$\frac{\partial T_s}{\partial t} = D_T\nabla^2 T_s, \quad \frac{\partial T_l}{\partial t} + (\mathbf{w},\nabla)\,T_l = D_T\nabla^2 T_l\,, \tag{2}$$

where D_T is the thermal diffusivity, $\mathbf{w}$ is the fluid flow velocity, and t is the time.

The distribution of an impurity in the liquid part of the system is described by the convective diffusion equation (impurity diffusion inside the growing crystal is neglected):

$$\frac{\partial C_l}{\partial t} + (\mathbf{w},\nabla)\,C_l = D_C\nabla^2 C_l\,, \tag{3}$$

where C_l is the concentration of the dissolved impurity, and D_C is the impurity diffusion coefficient.

Conditions of equality between phase temperatures and the phase transition temperature, of temperature continuity, and of heat–mass balance are fulfilled at the moving interface:

$$T_l = T_{\rm int} - mC_l\,, \quad T_s = T_l\,,$$

$$Q\mathbf{vn} = D_T c_p(\nabla T_s - \nabla T_l)\,\mathbf{n}\,, \tag{4}$$

$$(1-k_0)\,C_l\mathbf{vn} + D_C\nabla C_l\,\mathbf{n} = 0\,, \tag{5}$$

where $\mathbf{vn}$ is the normal velocity of surface movements, c_p is the heat capacity, and k_0 and m are the impurity distribution and liquidus slope equilibrium coefficients, respectively. Notice that the first expression in Eqn (4) gives the relationship between temperature and concentration in the form of the liquidus line equation on the phase diagram.

Let us consider subsequent to paper [32] the flow of fluid at small Reynolds numbers. In this case, the velocity distribution in a fluid satisfies Oseen and continuity equations [71]:

$$U\frac{\partial \mathbf{w}}{\partial z} = -\frac{1}{\rho_l}\nabla p + \nu\nabla^2\mathbf{w}\,, \quad \nabla\mathbf{w} = 0\,. \tag{6}$$

Here, U is the incoming flow velocity far from the growing crystal, and ρ_l and ν are fluid density and kinematic viscosity coefficients, respectively. It is worth noting that although the Oseen approximation used in the equation of motion (6) makes it possible to take into account only the most important inertial terms, calculations yield sufficiently

accurate results (see, for instance, the classical problem of sphere motion in a viscous fluid [72]).

The statement of the above-formulated problem by equations (1)–(6) also implies that the coefficient of impurity distribution between phases k_0, impurity diffusion coefficient D_C, liquidus slope m, liquid phase density ρ_l, and kinematic viscosity ν are constants. Moreover, thermal diffusivities in the phases are assumed to be similar, which allows directly employing the available methods for the description of dendrite growth [73–75]. Such a simplified statement of the problem ensues from the fact that the difference between thermal diffusivities enters the 'empirical constant' of the condition being sought for the selection of the stable dendrite growth regime. These simplifications collectively permit us to make analytical calculations for the systems of nonlinear equations with hydrodynamic contributions.

3.1 Analytical solution for a parabolic dendrite

Let us assume that a two-dimensional parabolic dendrite grows with a constant rate V along the spatial z-axis (Fig. 6). The fluid flow far from the crystal is oriented parallel to the z-axis and opposite to the dendrite growth direction (the so-called incoming flow). Let us further introduce the parabolic coordinates ξ and η related to the Cartesian coordinates x and z by the expressions

$$x = \rho\sqrt{\xi\eta}\,, \quad z = \frac{\rho}{2}\,(\eta - \xi)\,, \tag{7}$$

where ρ is the dendrite tip diameter, and the phase boundary lies at the $\eta = 1$ level (generalization to a three-dimensional case is considered in Section 5.3 below).

Equations (6) allow determining fluid velocity components u_η and u_ξ in the parabolic coordinates (7). Taking into account the boundary conditions for liquid adhesion to the dendrite surface, the specified incoming flow velocity, and Ref. [32], the result can be written in the form

$$u_\eta = -\frac{f(\eta)}{2\sqrt{\xi+\eta}}\,, \quad u_\xi = \frac{\sqrt{\xi\eta}}{\sqrt{\xi+\eta}}\,\frac{\mathrm{d}f}{\mathrm{d}\eta}\,, \tag{8}$$

with the functions introduced as follows:

$$f(\eta) = 2(U+V)\sqrt{\eta} - 2Ug(\eta)\,,$$

$$g(\eta) = \sqrt{\eta}\,\frac{\operatorname{erfc}\sqrt{\eta\,\mathrm{Re}/2}}{\operatorname{erfc}\sqrt{\mathrm{Re}/2}} + \frac{\sqrt{2/(\pi\,\mathrm{Re})}}{\operatorname{erfc}\sqrt{\mathrm{Re}/2}}\left[\exp\left(-\frac{\mathrm{Re}}{2}\right) - \exp\left(-\frac{\eta\,\mathrm{Re}}{2}\right)\right], \tag{9}$$

and taking into consideration flow intensity depending on the Reynolds number $\mathrm{Re} = \rho U/\nu$.

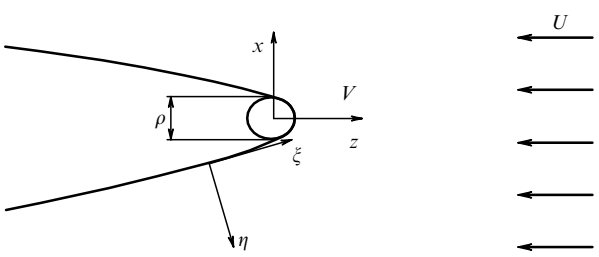

Figure 6. Schematic representation of a growing dendrite in the fluid counter flow, showing transformation to a new system of coordinates.

Equations (2) and (3) can be integrated in parabolic coordinates (7). To find the solution to the problem depending on η alone, Eqns (2) and (3) with boundary conditions (4) and (5) (see paper [31]) should be rewritten in the form

$$u_\eta\,\frac{\mathrm{d}T_l}{\mathrm{d}\eta} = \frac{2D_T}{\rho\sqrt{\xi+\eta}}\left(\sqrt{\eta}\,\frac{\mathrm{d}^2T_l}{\mathrm{d}\eta^2} + \frac{1}{2\sqrt{\eta}}\,\frac{\mathrm{d}T_l}{\mathrm{d}\eta}\right),$$

$$\left.\frac{\mathrm{d}T_l}{\mathrm{d}\eta}\right|_{\eta=1} = -\frac{Q}{c_p}\,\frac{\rho V}{2D_T}\,, \tag{10}$$

$$u_\eta\,\frac{\mathrm{d}C_l}{\mathrm{d}\eta} = \frac{2D_C}{\rho\sqrt{\xi+\eta}}\left(\sqrt{\eta}\,\frac{\mathrm{d}^2C_l}{\mathrm{d}\eta^2} + \frac{1}{2\sqrt{\eta}}\,\frac{\mathrm{d}C_l}{\mathrm{d}\eta}\right),$$

$$\left.\frac{\mathrm{d}C_l}{\mathrm{d}\eta}\right|_{\eta=1} = -(1-k_0)\,C_i\,\frac{\rho V}{2D_C}\,, \tag{11}$$

where C_i is the impurity concentration at the crystal–melt interface. Solving equations (10) and (11) yields the impurity temperature and concentration distributions:

$$T_l(\eta) = T_i + (T_\infty - T_i)\,\frac{I_T(\eta)}{I_T(\infty)}\,,$$

$$C_l(\eta) = C_i + (C_\infty - C_i)\,\frac{I_C(\eta)}{I_C(\infty)}\,. \tag{12}$$

Here, the following notations are introduced:

$$I_T(\eta) = \int_1^\eta \exp\left[P_f\int_1^{\eta'}\frac{g(\eta'')}{\sqrt{\eta''}}\,\mathrm{d}\eta'' - P_0\eta'\right]\frac{\mathrm{d}\eta'}{\sqrt{\eta'}}\,, \tag{13}$$

$$I_C(\eta) = \int_1^\eta \exp\left[P_f\,\frac{D_T}{D_C}\int_1^{\eta'}\frac{g(\eta'')}{\sqrt{\eta''}}\,\mathrm{d}\eta'' - P_0\,\frac{D_T}{D_C}\,\eta'\right]\frac{\mathrm{d}\eta'}{\sqrt{\eta'}}\,, \tag{14}$$

$$P_g = \frac{\rho V}{2D_T}\,, \quad P_f = \frac{\rho U}{2D_T}\,, \quad P_0 = P_f + P_g\,, \tag{15}$$

$$T_i = T_\infty + \frac{Q}{c_p}\,P_g\exp(P_0)\,I_T(\infty)\,, \tag{16}$$

$$C_i = \frac{C_\infty}{1-(1-k_0)\,\exp\left[P_0D_T/D_C\right]P_gI_C(\infty)\,D_T/D_C}\,, \tag{17}$$

where P_g and P_f are the growth and flow Péclet numbers, respectively, defined through the dendrite growth rate V and the fluid flow velocity U, and T_∞ and C_∞ are fluid temperature and concentration far from the interface, respectively.

3.2 Microscopic solvability condition

Surface energy anisotropy for various rapidly growing facets does not exceed 1.5–2.0% for traditional metals or alloys, and is up to 5.0% for strongly anisotropic crystalline materials. Given such a relatively small anisotropy of surface tension, solutions with a constant dendrite growth rate can be found in the neighborhood of classical solutions to Ivatsov's parabolic dendrite. Mathematically, this means the fulfillment of the microscopic solvability condition found as the approximate solution of the axisymmetric problem in the case of linearization of heat and mass transfer conditions on the Ivantsov dendrite surface [73, 74]. This condition allows selecting a stable growth regime in terms of velocity V and radius $\rho/2$ of the anisotropic dendrite tip (i.e., in the case of superimposed crystal lattice symmetry taking account of the anisotropy of

the predominant crystal growth direction) [28, 29]. In what follows, we shall utilize the microscopic solvability condition in the form [75]

$$\int_{-\infty}^{\infty} G\big[X_0(l)\big]\; Y_{\rm m}(l)\,{\rm d}l = 0\,,\;\; Y_{\rm m}(l) = \exp\left[{\rm i}\int_0^l k_{\rm m}(l_1)\,{\rm d}l_1\right]. \tag{18}$$

Expression (18) can be applied when analyzing various mobile boundaries, e.g., Saffman–Taylor 'viscous fingers' [28, 76]. It implies knowledge of curvature operator G and solutions $X_0(l)$ from which it is possible to find functions $k_{\rm m}(l)$ of the local nonzero marginal mode of the conjugate dispersion equation for perturbations (see, e.g., monograph [76]).

Relation (18) is derived with the aid of the Wentzel–Kramers–Brillouin (WKB) approximation [77] that was applied to obtain the flame front propagation regimes [78] and the dendritic structure [79]. Functions $Y_{\rm m}(l)$ in relation (18) in the presence of the incoming flow of a viscous binary fluid are defined in Section 5.

4. Linear stability analysis

Stability analysis in the linear approximation permits determining the dendritic surface reaction near the tip to a small perturbation. Finding stability, instability, and marginal (borderline) state regions depending on the perturbation wave number is the main purpose of the analysis. The marginal mode (the borderline regime between stability and instability) is found from the critical value of wave number $k_{\rm m}$ corresponding to the neutral stability curve. To obtain this critical value at the dendrite tip, we now turn to the results of linear stability analysis from Ref. [32], in which the perturbation growth rate had a wavelength much shorter than the characteristic spatial scale of the unperturbed solution.

Let us expand the stationary velocity components (8) in a power series of $\eta - 1$ on the outskirts of the parabola set by the equation $\eta = 1$. Taking into account only the main contributions, we arrive at

$$u_\xi = \sqrt{\frac{\xi}{1+\xi}}\big[V + a({\rm Re})\,U(\eta-1)\big]\,,\quad u_\eta = -\frac{V}{\sqrt{1+\xi}}\,, \tag{19}$$

where

$$a({\rm Re}) = \sqrt{\frac{\rm Re}{2\pi}}\,\frac{\exp\left(-{\rm Re}/2\right)}{{\rm erfc}\left(\sqrt{{\rm Re}/2}\right)}. \tag{20}$$

It follows from formulas (19) and (20) that only the tangent velocity component u_ξ is dependent on the incoming flow velocity close to the parabolic tip of the growing dendrite.

For further analysis, we will introduce new local Cartesian coordinates $x_{\rm c}$ and $y_{\rm c}$ fixed to the crystal, which specify the tangent and normal axes, respectively, to the interface at a point where the normal to the latter makes an angle θ with the growth axis. These coordinates allow us to represent expressions (19) through $\theta_{\rm c}$ and $y_{\rm c}$:

$$\overline{u} = -V\sin\theta - \frac{aU}{\rho}\,y_{\rm c}\sin\theta\cos\theta\,,\qquad \overline{v} = -V\cos\theta\,, \tag{21}$$

where $\overline{u}$ and $\overline{v}$ denote the tangent and normal velocity components near the dendrite surface, respectively. Expressing the derivatives of temperature and concentration from Eqns (4) and (5) as

$$\frac{{\rm d}\overline{T_{\rm l}}}{{\rm d}y_{\rm c}} = \frac{Q\overline{v}}{D_T c_p}\,,\qquad \frac{{\rm d}\overline{C_{\rm l}}}{{\rm d}y_{\rm c}} = \frac{C_{\rm i}(1-k_0)\,\overline{v}}{D_C}\quad \text{at } y_{\rm c} = 0 \tag{22}$$

yields an expansion in a power series for temperature and concentration in the vicinity of the dendrite tip:

$$\overline{T_{\rm l}} = T_{\rm i} - \frac{QV}{D_T c_p}\,y_{\rm c}\cos\theta\,,\quad \overline{C_{\rm l}} = C_{\rm i} - \frac{C_{\rm i}(1-k_0)\,V}{D_C}\,y_{\rm c}\cos\theta\,. \tag{23}$$

Letting u', v', and T' designate perturbations of the respective quantities, and ξ' perturbation of the stationary interface with a wavelength λ assumed very small compared to radius $\rho/2$ of the dendrite tip enables one to represent the solution of equations for perturbations obtained from equations (2) and (6) in the Oseen approximation in the form (see also paper [32])

$$\begin{aligned}
u' &= (B - {\rm i}\varepsilon A y_{\rm c})\exp\left(\omega t + {\rm i}kx_{\rm c} - \varepsilon k y_{\rm c}\right),\\
v' &= \left[A\left(y_{\rm c} + \frac{\varepsilon}{k}\right) + {\rm i}B\varepsilon\right]\exp\left(\omega t + {\rm i}kx_{\rm c} - \varepsilon k y_{\rm c}\right),\\
\xi' &= \Sigma\exp\left(\omega t + {\rm i}kx_{\rm c} - \varepsilon k y_{\rm c}\right),\\
A &= -\Sigma\left(\omega k\varepsilon + {\rm i}\,\frac{akU}{\rho}\sin\theta\cos\theta\right),\\
B &= \Sigma\,\frac{aU}{\rho}\sin\theta\cos\theta\,,
\end{aligned} \tag{24}$$

where the equality $v' = -\partial\xi'/\partial t$ fulfilled at the interface was taken into consideration. Here, ω and k are the increment and the wave number of the perturbations, respectively, parameter ε has the same sign as the real part of k since perturbations cannot increase unrestrictedly as $y_{\rm c}$ goes to ∞, and Σ is the perturbation amplitude of the dendrite surface.

Let us address the equation for temperature perturbations in the liquid part of the system. Keeping up only linear terms, one obtains from equation (2):

$$\frac{\partial T_{\rm l}'}{\partial t} + \overline{u}\frac{\partial T_{\rm l}'}{\partial x_{\rm c}} + \overline{v}\frac{\partial T_{\rm l}'}{\partial y_{\rm c}} + v'\,\frac{{\rm d}\overline{T_{\rm l}}}{{\rm d}y_{\rm c}} = D_T\left(\frac{\partial^2 T_{\rm l}'}{\partial x_{\rm c}^2} + \frac{\partial^2 T_{\rm l}'}{\partial y_{\rm c}^2}\right). \tag{25}$$

If the velocity of an incoming flow is negligible, the solution has a form similar to $T_{\rm l}' = T_{\rm l0}\exp\left(\omega t + {\rm i}kx_{\rm c} - \varepsilon k y_{\rm c}\right)$ at large k, $T_{\rm l0} \equiv {\rm const}$, consistent with the well-known Mullins–Sekerka criterion [24] at k determined within the domain boundaries of the thermal problem for one-component liquid solidification (see Ref. [32] among others). Substituting

$$T_{\rm l}' = g(y_{\rm c})\,\exp\left(\omega t + {\rm i}kx_{\rm c} - \varepsilon k y_{\rm c}\right) \tag{26}$$

into equation (25) and taking into account formulas (22), (23) lead to the following equation for the $g(y_{\rm c})$ amplitude:

$$\frac{{\rm d}^2 g}{{\rm d}y_{\rm c}^2} - 2\varepsilon k\,\frac{{\rm d}g}{{\rm d}y_{\rm c}} = L\big(g(y_{\rm c}), y_{\rm c}\big)\,, \tag{27}$$

where

$$\begin{aligned}
L\big(g(y_{\rm c}), y_{\rm c}\big) &= \frac{\Sigma QV\cos\theta}{c_p D_T^2}\left[\omega + (\omega k\varepsilon + kN)\,y_{\rm c}\right]\\
&\quad + \left[\frac{\omega + kV(\varepsilon\cos\theta - {\rm i}\sin\theta)}{D_T} - \frac{kNy_{\rm c}}{D_T}\right]g(y_{\rm c})\,,
\end{aligned} \tag{28}$$

$$N = \frac{{\rm i}aU\sin\theta\cos\theta}{\rho}\,.$$

To solve the set of equations (27), (28), we will apply the method proposed in paper [32]. Because g varies on scale λ, the left-hand side of equation (27) prevails over its right-hand side at large wave numbers, thus allowing the system (27), (28) to be solved by expanding the solution at large k. The zero approximation yields $g = T_{l0}$, where T_{l0} is the constant amplitude. Substituting it into the right-hand side of formula (28) gives the solution of equation (27) in the form

$$g(y_c) = T_{l0} + T_{l1} y_c + T_{l2} y_c^2 ,$$

$$T_{l1} = \left[\frac{N}{4} - \frac{\omega + Vk(\varepsilon \cos\theta - i \sin\theta)}{2\varepsilon} \right] \frac{T_{l0}}{kD_T} - \frac{\Sigma Q V \cos\theta}{4kD_T^2 c_p} (3\omega\varepsilon + N) , \quad (29)$$

where the strong inequality $V/D_T \ll k$ was taken into consideration, with k being estimated from the Mullins–Sekerka theory as $\sim 10^6 - 10^7$ m^{-1} [24], and V/D_T as $\sim 10^2$ m^{-1} for binary metallic alloys.

Equation (3), written for concentration field perturbations C_l' in the liquid, can be solved in the same manner. The result is written out as

$$C_l' = (C_{l0} + C_{l1} y_c + C_{l2} y_c^2) \exp(\omega t + ikx_c - \varepsilon k y_c) ,$$

$$C_{l1} = \left[\frac{N}{4} - \frac{\omega + Vk(\varepsilon \cos\theta - i \sin\theta)}{2\varepsilon} \right] \frac{C_{l0}}{kD_C} - \frac{\Sigma C_i (1 - k_0) V \cos\theta}{4kD_C^2} (3\omega\varepsilon + N) . \quad (30)$$

The expressions for perturbation amplitudes T_{l2} and C_{l2} are not presented here, as they are unnecessary for further analysis. The equation for solid phase temperature is solved in a similar manner, and its solution is expressed in the form (29) at $U = 0$.

Now, perturbing the boundary conditions (4) and (5), we arrive at the following set of equations at the solid–liquid interface $y_c = 0$:

$$T_l' = \frac{QV\cos\theta}{D_T c_p} \xi' - mC_l' + \frac{mC_i(1 - k_0) V \cos\theta}{D_C} \xi' - \frac{Qd}{c_p} \frac{\partial^2 \xi'}{\partial y_c^2} ,$$

$$T_s' = mC_l' - \frac{mC_i(1 - k_0) V \cos\theta}{D_C} \xi' + \frac{Qd}{c_p} \frac{\partial^2 \xi'}{\partial y_c^2} ,$$

$$\frac{1 - k_0}{D_C} (C_i v' - C_l' V \cos\theta) = \frac{\partial C_l'}{\partial y_c} + \frac{C_i k_0 (1 - k_0) V^2 \cos^2\theta}{D_C^2} \xi' ,$$

$$\frac{Q}{c_p} \frac{\partial \xi'}{\partial t} = D_T \left(\frac{\partial T_s'}{\partial y_c} - \frac{\partial T_l'}{\partial y_c} - \frac{QV^2 \cos^2\theta}{D_T^2 c_p} \xi' \right) , \quad (31)$$

where $d = \sigma c_p T_0 / Q^2$ stands for the capillary length.

Substitution of perturbations (24), (26), and (30) into the boundary conditions (31) gives four linear equations for the perturbation amplitudes Σ, T_{l0}, T_{s0}, and C_{l0} (where T_{s0} is the constant amplitude of temperature perturbation in the solid phase). The zero value of the determinant of this set of equations accounts in its turn for dispersion relation $\omega(k)$.

Let us consider a reference frame, the origin of which moves normally to the interface at velocity $V \cos\theta$. Because of the rotational symmetry of the system, a perturbation with the wave number k grows at the rate $\omega(k)$. If the origin of the frame moves in the direction of the z-axis with a constant velocity V, the perturbation growth rate will take the form $\omega(k) - iVk \sin\theta$ due to the present of the tangential velocity $V \sin\theta$ in the new reference frame [33]. Therefore, replacing $\omega(k) \to -iVk \sin\theta$ in the neutral stability curve (where $\omega = 0$), eliminating the perturbation amplitudes, assuming $\varepsilon = -1$, and substituting $-i$ for i lead, in accordance with Ref. [32], to the equation for the marginal mode of the wave number $k = k_m$:

$$k^2 = \left(\frac{V}{2dD_T} + \frac{mC_i(1 - k_0) V c_p}{dD_C Q} \right) \exp(i\theta) + i \frac{aU \sin\theta \cos\theta}{8\rho D_T} + i \frac{aU \sin\theta \cos\theta}{4\rho D_C} . \quad (32)$$

Expression (32) is written out taking account of the following estimates: $k \sim 10^6 - 10^7$ m^{-1}, $V/D_T \sim 10^2$ m^{-1}, $V/D_C \sim 10^6$ m^{-1}, $d \sim 10^{-9} - 10^{-10}$ m, and $\rho \sim 10^{-5}$ m. This expression defines the critical value of k_m that separates the unstable and stable mode regions of the wave number.

Let us represent the capillary length as $d(\theta) = d_0[1 - \beta \cos(4\theta)]$ (where $\beta = 15\varepsilon_c \ll 1$ is the anisotropy factor, ε_c is the parameter of surface energy anisotropy at the interface, and d_0 is the capillary constant), and then introduce the wave number

$$k_{TC} = -\left(\frac{VP}{2d_0 D_T} \right)^{1/2} , \quad P = 1 + \frac{2mC_i(1 - k_0) D_T}{D_C Q / c_p} , \quad (33)$$

corresponding to the solution of the thermoconcentration problem in the absence of a flow (see, for instance, paper [33]). After these manipulations, the solution of equation (32) takes the form

$$k = k_{TC} \left(\frac{\exp(i\theta) + i\alpha [1 - \beta \cos(4\theta)] \sin\theta \cos\theta}{1 - \beta \cos(4\theta)} \right)^{1/2} , \quad (34)$$

where

$$\alpha = \frac{ad_0 U}{4\rho VP} + \frac{ad_0 U D_T}{2\rho VP D_C} , \quad (35)$$

and P is given by formula (33).

Expressions (32) and (34) contain limiting transformations to the earlier theories of dendrite growth with anisotropic surface energy [24, 32, 33, 75, 76]. Assuming first $U = 0$ and $C_i = 0$ in equation (32) or (34) gives the Mullins–Sekerka wave number k_{MS} for a one-component stagnant fluid [24, 32, 75, 76]:

$$k_{MS} = -\sqrt{\frac{V \exp(i\theta)}{2dD_T}} . \quad (36)$$

Next, solution (32) [and accordingly (34)] leads at $U = 0$ to the wave number k_{BAP} obtained by Ben Amar and Pelcé for a stagnant binary fluid [33]:

$$k_{BAP} = k_{MS} \sqrt{P} . \quad (37)$$

Now, assuming $D_C \to \infty$, we arrive at the solution for k_{BP} obtained by Bouissou and Pelcé for a one-component system

in the presence of a counter flow of fluid [32]:

$$k_{\mathrm{BP}} = k_{\mathrm{MS}}\sqrt{1+\frac{\mathrm{i}adU\sin\theta\cos\theta\exp(-\mathrm{i}\theta)}{4\rho V}}. \tag{38}$$

Expressions (37) and (38) disseminate the results of paper [54] to concentrated binary liquids in the presence of a counter flow of fluid.

It should be particularly noted that relations (32) and (34) also lead to a new result describing dendrite growth in an isothermal binary system in the presence of a counter flow of fluid, which gives rise to the growth of so-called chemical dendrite. Assuming $D_T \to \infty$ in expressions (32) or (34) leads to the wave number k_{CD} for the chemical dendrite:

$$k_{\mathrm{CD}} = -\sqrt{K_{\mathrm{chem}}}\,,$$
$$K_{\mathrm{chem}} = \frac{V}{d_0 D_C}\left\{\frac{mC_{\mathrm{i}}(1-k_0)\,c_p}{Q[1-\beta\cos(4\theta)]}\exp(\mathrm{i}\theta) + \frac{\mathrm{i}aUd_0\sin\theta\cos\theta}{4\rho V}\right\}. \tag{39}$$

Bearing in mind that $d = d_0[1-\beta\cos(4\theta)] = \sigma c_p T_0/Q^2$, relation (39) can be rewritten as

$$k_{\mathrm{CD}} = k_{\mathrm{d}}\left[1+\frac{\mathrm{i}ad_{\mathrm{CD}}U\sin\theta\cos\theta\exp(-\mathrm{i}\theta)}{2\rho V}\right]^{1/2}, \tag{40}$$

where the wave number k_{d} characterizing the solution to the diffusion problem for a chemical dendrite without a flow and the chemical capillary length d_{CD} are defined by the relations

$$k_{\mathrm{d}} = -\sqrt{\frac{V\exp(\mathrm{i}\theta)}{2d_{\mathrm{CD}}D_C}}, \quad d_{\mathrm{CD}} = \frac{\sigma T_0}{2QmC_{\mathrm{i}}(1-k_0)}\,. \tag{41}$$

The wave number k_{CD} given by expression (40) for an isothermal dendrite in a binary system with a flow and the wave number k_{BP} defined by expression (38) for a thermal dendrite in a one-component system with a flow have a qualitatively similar form ensuing directly from analysis of the terms of the more general equation (32). The quantitative difference between k_{BP} (38) and k_{CD} (40) is due to the fact that the pure concentration problem, unlike the temperature one, is solvable only in the liquid phase domain (the authors of Ref. [33] called this case a 'one-sided model'). Such an asymmetry in solutions of the two statements of the problem has already been reflected in formula (32) and passes to expressions for the wave numbers k_{CD} and k_{BP} in the form of factor 2.

Thus, the generalized solution (34) gives the critical wave number for perturbations at the dendritic tip in the framework of the mass and heat transfer problem taking account of the counter flow of fluid.

5. Stability criterion for dendritic tip

We make use of the selection theory developed in Refs [32, 75, 76] to obtain the stability criterion for dendritic tip growth. Bearing in mind that the integration variable l in the microscopic solvability conditions (18) is related to angle θ as

$$l = -\frac{\rho}{2}\left[\frac{\tan\theta}{\cos\theta}+\ln\left(\frac{1}{\cos\theta}+\tan\theta\right)\right]$$

(see, for example, paper [75]), we write down the solvability condition (18) by analogy with Ref. [32] in the form

$$\int_{-\infty}^{\infty} G[(\chi)]\exp\left[\sqrt{C}\,\Psi_\alpha(\chi)\right]\mathrm{d}\chi = 0\,, \quad \chi = \tan\theta\,, \tag{42}$$

showing that curvature operator $G[(\chi)]$ acts on function χ:

$$\Psi_\alpha(\chi) = \frac{\mathrm{i}}{2}\int_0^\chi \frac{\left[(1+\mathrm{i}\chi')(1+\chi'^2)^{5/2}+\mathrm{i}\alpha\chi' B(\chi')\right]^{1/2}}{\sqrt{B(\chi')}}\,\mathrm{d}\chi'\,,$$
$$B(\chi) = (1+\chi^2)^2(1-\beta)+8\beta\chi^2\,, \tag{43}$$

while constant C is normalized to the dimensionless factor $VP\rho^2/(2d_0D_T)$.

Let us evaluate integral (43) in the limit of small anisotropy by the method developed in Ref. [32]. The numerator of the integrand vanishes at χ close to $\chi = \mathrm{i}$ (stationary phase point), and the denominator at $\chi = \mathrm{i}(1-\sqrt{2\beta})$ (point of singularity). Since the dominant contribution to the integral is determined by the neighborhood of the point $\chi = \mathrm{i}$, function $\Psi_\alpha(\chi)$ can be approximated by

$$\Psi_\tau(\varphi) = 2^{9/8}\beta^{7/8}\int_{1/\sqrt{2\beta}}^{\varphi}\frac{\left[\varphi'^{7/2}-\tau(\varphi'^2-1)\right]^{1/2}}{\sqrt{\varphi'^2-1}}\,\mathrm{d}\varphi', \tag{44}$$

where

$$\chi = \mathrm{i}\left(1-\sqrt{2\beta}\varphi\right), \quad \tau = 2^{-5/4}\beta^{-3/4}\alpha\,.$$

Integral (44) can be approximately calculated by the methods developed in Ref. [32] for the analysis of a similar problem of the dendrite growth in a one-component system with a convective flow. Based on the results of this analysis, the quantity C is defined as

$$C = \frac{n^2}{\beta^{7/4}}\left[1+b(\beta^{-3/4}\alpha)^{11/14}\right], \tag{45}$$

where n is an integer, and b is a numerical constant. Now, taking account of the normalization in integral (44) leads to the expression for the scaling factor σ^* of the heat and mass transfer problem with a fluid flow:

$$\sigma^* \equiv \frac{2d_0D_T}{\rho^2 V} = \sigma_0\beta^{7/4}P\left[1+b(\beta^{-3/4}\alpha)^{11/14}\right]^{-1}. \tag{46}$$

Here, σ_0 is the numerical constant determined with the aid of asymptotic methods [29] or by fitting the model results to available experimental data [80, 81]. The scaling factor σ^* describes the relationship between velocity V and tip radius $\rho/2$ under the stable growth regime of parabolic dendrite trunk. Expression (46), together with the supercooling balance at the phase boundary, quantitatively defines V and ρ (see Section 6.2.2).

5.1 Limiting cases and the role of convection

In the case of dendrite growth in a one-component system under convection, the Bouissou–Pelcé scaling factor [32] is obtained from formula (46) as the limit for $D_C \to \infty$, when $\alpha \to \alpha_{\mathrm{BP}} \equiv ad_0U/(4\rho V)$ and $P \to 1$:

$$\sigma^*_{\mathrm{BP}} = \sigma_0\beta^{7/4}\left[1+b(\beta^{-3/4}\alpha_{\mathrm{BP}})^{11/14}\right]^{-1}. \tag{47}$$

The scaling factor for a 'concentration' dendrite (i.e., 'chemical' or 'solutal' crystal growing in an isothermal liquid) is easy to derive from expression (46):

$$\sigma^*_{\rm CD} \equiv \frac{2d_{0\rm CD}D_C}{\rho^2 V} = \sigma_0 \beta^{7/4}\left[1 + b(\beta^{-3/4}\alpha_{\rm CD})^{11/14}\right]^{-1}, \quad (48)$$

where

$$\alpha_{\rm CD} = \frac{ad_{0\rm CD}U}{2\rho V}, \quad d_{0\rm CD} = \frac{Qd_0}{2mC_{\rm i}(1-k_0)\,c_p}. \quad (49)$$

The relationship between capillary constants $d_{0\rm CD}$ and d_0 in expressions (46), (48), and (49) ensues from formulas

$$d_{\rm CD} = \frac{\sigma T_0}{2QmC_{\rm i}(1-k_0)} = d_{0\rm CD}\left[1 - \beta\cos(4\theta)\right],$$

$$d = \frac{\sigma T_0 c_p}{Q^2} = d_0\left[1 - \beta\cos(4\theta)\right]. \quad (50)$$

Worthy of mention is a similar form of expressions for scaling factors $\sigma^*_{\rm CD}$ (see factor (48) for an isothermal dendrite in a binary system with a fluid flow) and $\sigma^*_{\rm BP}$ (see factor (47) for a thermal dendrite in a one-component system with a fluid flow). These expressions are totally identical in terms of structure, just like the expressions for the wave numbers $k_{\rm CD}$ and $k_{\rm BP}$ discussed in Section 4.

Expressions (46) and (47) define criteria for the stable mode of dendritic tip growth taking account of surface energy anisotropy (parameter β), nonisothermicity of the binary system, and the incoming flow of fluid. Criterion (46) integrates certain earlier results, such as the model from Ref. [32] for a nonisothermal one-component system with an incoming fluid flow, and the model from Ref. [33] for an isothermal binary system taking no account of the counter flow of fluid. In other words, relation (46) serves as the generalization of the earlier obtained criteria for the selection of stable dendrite growth regimes.

Let us evaluate the influence of convection on the selection criterion for the stable dendritic growth regime. To this effect, stability criterion (46) needs to be estimated with respect to the criterion without convection:

$$\frac{\sigma^*}{\sigma^*|_{\alpha=0}} = \left[1 + b(\beta^{-3/4}\alpha)^{11/14}\right]^{-1}, \quad (51)$$

where α is given as in expression (35), $\sigma^*|_{\alpha=0}$ is determined for the dendrite growth in the absence of a flow, namely

$$\sigma^*|_{\alpha=0} = \sigma_0\beta^{7/4}P, \quad (52)$$

and P is given by formula (33). Figure 7 displays the dependence of the dendritic tip stability criterion on the growth Peclét number at different convective flow intensities given by the flow Peclét number $P_{\rm f}$. Evidently, a decrease in $P_{\rm f}$ corresponding to the fluid flow, and an increase in $P_{\rm g}$ corresponding to the dendrite growth result in a reduced contribution of convection to the stability of the dendritic tip growth.

5.2 Estimation of dendrite growth stability from experimental data

The values of parameters b and σ_0 in the generalized criterion (46) for stable dendrite growth can be derived from natural experiments. Indeed, experiments on the growth of dendrites

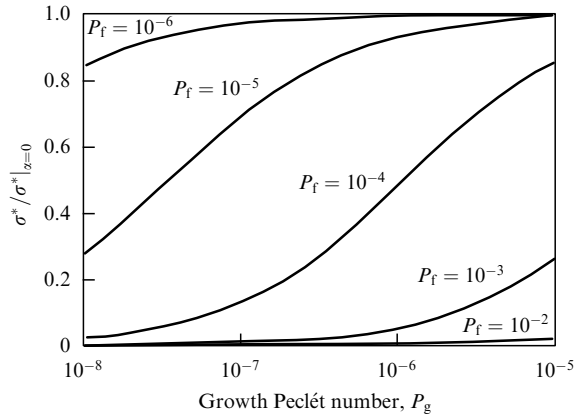

Figure 7. Ratio $\sigma^*/\sigma^*|_{\alpha=0}$ obtained from expressions (51) and (52) as a function of the growth Peclét number $P_{\rm g} = V\rho/(2D_T)$ for different values of the flow Peclét number $P_{\rm f} = U\rho/(2D_T)$ and the parameters $D_T/\nu = 10$, $d_0/\rho = 10^{-5}$, $\beta = 0.195$, $D_T/D_C = 5\times10^3$, $k_0 = 0.5$, $C_\infty = 0.01$ at.%, $m = 10$ K (at.%)$^{-1}$, $Q/c_p = 300$, and $b = 10$.

into trimethylacetic acid under convection [82] showed that product $\rho^2 V$ is a constant depending only on the counter flow velocity of the melt. The experimental value of this product can be written down as [82]

$$(\rho^2 V)_{\rm exp} = 2\sigma^{-1}_{\rm exp} d_0 D_C\left(1 + \chi_{\rm exp}\frac{Ud_0}{D_C}\right), \quad (53)$$

where $\sigma_{\rm exp} \approx 0.032$, and $\chi_{\rm exp} \approx 5300$. Exponent 11/14 in expressions (46) and (48) is rather close to unity, which makes it difficult to see the difference between these quantities using current experimental techniques [32]. Therefore, the product $\rho^2 V$ from formula (48) can be approximately represented as

$$\rho^2 V = \frac{2d_0 D_C}{\beta^{7/4}\sigma_{\rm CD}}\left(1 + b\beta^{-3/4}\alpha_{\rm CD}\right), \quad (54)$$

$$\sigma_{\rm CD} = 2mC_{\rm i}(1-k_0)\,c_p\,\frac{\sigma_0}{Q}.$$

A comparison of expressions (53) and (54) yields unknown coefficients

$$\sigma_{\rm CD} \approx \frac{\sigma_{\rm exp}}{\beta^{7/4}}, \quad b \approx \frac{4\rho V m C_{\rm i}(1-k_0)\,\chi_{\rm exp}\,\beta^{3/4}c_p}{a({\rm Re})\,D_C Q}, \quad (55)$$

where function $a({\rm Re})$ is given by expression (20).

Notice that parameters σ_0 and b from formulas (55) are determined at all other fixed parameters of dendrite growth in trimethylacetic acid, as described in Ref. [82]. Thus, parameters entering the stability criterion can be evaluated from experimental data.

5.3 Dendrite growth under convection in a three-dimensional space

The above analysis qualitatively holds true for three-dimensional dendritic growth. Let us introduce the coordinates of a paraboloid of revolution whose z-axis coincides with the z-axis for a plane case described by relation (7):

$$z = \frac{\rho(\eta - \xi)}{2}, \quad x = \rho\sqrt{\xi\eta}\cos\varphi, \quad y = \rho\sqrt{\xi\eta}\sin\varphi, \quad (56)$$

where the dendrite surface $\eta = 1$ has the tip radius $\rho/2$ as before, and φ is the polar angle in the plane perpendicular to the incoming fluid flow along the z-axis. In this case, the fluid velocity components take the form analogous to expressions (8):

$$u_\eta = -\frac{f(\eta)}{\sqrt{\xi+\eta}}\,, \quad u_\xi = \sqrt{\frac{\xi}{\xi+\eta}}\,\frac{\mathrm{d}}{\mathrm{d}\eta}\left(\sqrt{\eta}\,f(\eta)\right), \quad u_\varphi = 0\,, \tag{57}$$

with the functions introduced as follows:

$$f(\eta) = (U+V)\sqrt{\eta} - 2Ug(\eta)\,,$$

$$g(\eta) = \frac{\sqrt{\eta}\,\mathrm{E}_1(\mathrm{Re}\,\eta/2)}{2\mathrm{E}_1(\mathrm{Re}/2)} + \frac{\exp(-\mathrm{Re}/2) - \exp(-\mathrm{Re}\,\eta/2)}{\sqrt{\eta}\,\mathrm{Re}\,\mathrm{E}_1(\mathrm{Re}/2)}\,,$$

$$\mathrm{E}_1(q) = \int_q^\infty \frac{\exp(-u)}{u}\,\mathrm{d}u\,. \tag{58}$$

The temperature and concentration fields are described as before by expressions (12), in which integrals (13) and (14) assume now the form

$$I_T(\eta) = \int_1^\eta \exp\left[2P_\mathrm{f}\int_1^{\eta'}\frac{g(\eta'')}{\sqrt{\eta''}}\,\mathrm{d}\eta'' - P_0\eta'\right]\frac{\mathrm{d}\eta'}{\eta'}\,, \tag{59}$$

$$I_C(\eta) = \int_1^\eta \exp\left[2P_\mathrm{f}\,\frac{D_T}{D_C}\int_1^{\eta'}\frac{g(\eta'')}{\sqrt{\eta''}}\,\mathrm{d}\eta'' - P_0\,\frac{D_T}{D_C}\,\eta'\right]\frac{\mathrm{d}\eta'}{\eta'}\,, \tag{60}$$

where P_0 is defined by formula (15).

The velocity components (19) for three-dimensional space remain unaltered, too; only coefficient $a(\mathrm{Re})$ depending on the Reynolds number changes. Indeed, there appears the relation

$$a(\mathrm{Re}) = \frac{\exp(-\mathrm{Re}/2)}{\mathrm{E}_1(\mathrm{Re}/2)} \tag{61}$$

instead of expression (20) for the three-dimensional case.

All other expressions of the linear stability theory (see Section 4) contain only dependence on coefficient $\alpha(\mathrm{Re})$. Therefore, expressions (34), (46), and (48) presenting the main result of our analysis are conserved in the three-dimensional case after the substitution of dependence (61) for the coefficient $a(\mathrm{Re})$.

5.4 Remarks. Special aspects and extension of the theory

Oseen equations (6) for the approximate description of hydrodynamic transport hold, generally speaking, at small Reynolds numbers (therefore, at the small flow Peclét number P_f). This approximation is applied to obtain an analytical solution to the problem of viscous fluid flowing around a dendrite. The theory provides another analytical solution to the parabolic dendrite problem, obtained using the ideal fluid model [31]. This solution holds for $\mathrm{Re} \gg 1$ and has, according to Ref. [31], the following form in the two-dimensional case:

$$u_\eta = -\frac{(U+V)\sqrt{\eta} - U}{\sqrt{\xi+\eta}}\,, \quad u_\xi = \sqrt{\frac{\xi}{\xi+\eta}}\,(U+V)\,. \tag{62}$$

Thus, the solution for two asymptotic cases is known, viz. expressions (8) hold for $\mathrm{Re} = \rho U/\nu \ll 1$, and expressions (62) for $\mathrm{Re} \gg 1$. The natural question arises concerning the form of the solution for the problem of interest in the case of all remaining Reynolds numbers.

To estimate the validity limit of the above solutions, it should be borne in mind that expressions (8) for a viscous liquid transform into expressions (62) for an ideal fluid at $g = 1$. Function g, formally dependent on the Reynolds number, $g = g(\eta, \mathrm{Re})$, tends toward unity with its rise (as $\mathrm{Re} \to \infty$) for the fixed values of coordinate $\eta > 1$. This means that solutions (8) found at small Reynolds numbers transform into solutions (62) for large Reynolds numbers. Because the Oseen approximation [hence, formulas (8)] is in excellent agreement with the numerical solution of the Navier–Stokes equations at Reynolds numbers up to $\mathrm{Re} \sim 1$ [30], formulas (8) can be regarded as adequately describing the process over a wide range of Re values, from small to large ones. This was confirmed in Ref. [83] reporting that a theoretical description of the flow in the Oseen approximation is consistent with experimental data at large Reynolds numbers. Similar reasoning also holds for the three-dimensional problem. It lifts the formal constraints in terms of flow Reynolds $\mathrm{Re} = \rho U/\nu$ and Peclét $P_\mathrm{f} = \rho U/(2D_T)$ numbers, narrowing the scope of applicability of the theory in question for an incoming laminar flow.

Two important remarks as regards the theory being considered are in order.

First, criteria (46) and (48) for stable dendrite growth in a binary system under convection can be tested for compliance with the results of computer simulation. Such testing is possible by the phase field method for free space dendrite growth with convection in a one-component system [42, 84]. Also, the stability criteria thus obtained can be verified experimentally as in the case of dendrite growth under forced flow of a transparent fluid [60].

Second, the application of criteria (46) and (48) is limited by the relatively small values of the growth Peclét number $P_\mathrm{g} = \rho V/(2D_T)$. In other words, the results of the analysis of dendritic growth hold only for small gradients or supercoolings of the liquid, maintaining low growth rates V of dendritic crystals. For the purpose of extended analysis at high growth rates and arbitrary Peclét numbers P_g, the stability of high-speed dendrite solidification regimes needs to be specially considered. The microscopic solvability condition for the high-speed growth regime can be obtained and analyzed in analogy with the same operations in the framework of the marginal stability hypothesis [85, 86]. Specifically, the selection criterion for dendrite growth in the problem of heat and mass transfer with convection and surface tension anisotropy at arbitrary Peclét numbers was determined in Ref. [87]:

$$\sigma^* = \frac{\sigma_0\beta^{7/4}}{1 + b(\alpha\beta^{-3/4})^{11/14}}\left[\frac{1}{(1 + a_1\sqrt{\beta}\,P_\mathrm{g})^2}\right.$$

$$\left. + \frac{1}{(1 + a_2\sqrt{\beta}\,P_\mathrm{g}D_T/D_C)^2}\,\frac{2mC_\mathrm{i}(1-k_0)\,D_T}{(Q/c_p)\,D_C}\right], \tag{63}$$

where constants a_1 and a_2 have the form

$$a_1 \approx 0.381\sigma_0^{1/2}\,, \quad a_2 \approx 0.505\sigma_0^{1/2}\,,$$

while parameters P and α are given by expressions (33) and (35), respectively. Constants σ_0 and b entering stability criterion (63) can be obtained by asymptotic analysis and simulation by the phase field method [42, 84], or from experimental data [82] (see Section 5.2). Generalized stability criterion (63) differs from (46) by the presence of the additional quadratic dependence on the growth Peclét number in the contributions from heat and matter transfer [see the denominators in parentheses on the right-hand side of formula (63)]. This dependence qualitatively and quantitatively modifies the behavior of the dendrite tip radius and the growth rate at elevated values of the growth Peclét number [87].

This theory can be utilized to obtain the rate of stable dendritic growth in multicomponent systems. By way of example, there is criterion σ^* obtained in Ref. [88] in the absence of convection:

$$\sigma^* = \frac{2d_0 D_T}{\rho^2 V} = \sigma_0 \beta^{7/4} \left[1 + 2\,\frac{D_T c_p}{Q} \sum_{j=1}^{N} \frac{m_j C_{ij}(1-k_{0j})}{D_{Cj}} \right], \tag{64}$$

where N is the number of impurity components, and m_j, C_{ij}, k_{0j}, and D_{Cj} are the liquidus slope coefficient, surface concentration, impurity distribution coefficient, and diffusion coefficient of the jth impurity component, respectively.

Stability criteria (63) and (64) can be reduced to a single criterion by the methods developed in Ref. [87]. This criterion defining conditions for stable dendritic tip growth in a nonisothermal many-component system under convection at arbitrary Reynolds (in the laminar flow region) and Peclét numbers has the form

$$\sigma^* = \frac{\sigma_0 \beta^{7/4}}{1 + b(\alpha\beta^{-3/4})^{11/14}} \left[\frac{1}{(1 + a_1 \sqrt{\beta}\, P_g)^2} + 2\,\frac{D_T c_p}{Q} \sum_{j=1}^{N} \frac{m_j C_{ij}(1-k_{0j})}{D_{C_j}(1 + a_2 \sqrt{\beta}\, P_g D_T / D_{C_j})^2} \right]. \tag{65}$$

The theory can be extended to a description of the growth of dendritic crystal-like structures on the surface of Earth's solid core. In this case, analysis of microscopic solvability should take account of the influence of pressure and the smallness of the Peclét number [89]. The criterion for stable crystal growth reported in paper [89] establishes the relationships among the thermophysical properties of the liquid–solid interface in Earth's core and allows quantitatively estimating the dynamic viscosity coefficient of the liquid core.

6. Quantitative evaluation of the model

6.1 Model for determining dendritic tip growth rate and radius

Let us construct, based on the theory expounded in Sections 3–5, a model for determining the main parameters of the dendrite growth, viz. tip growth rate and radius. Let us consider for this purpose a dendrite growing at a rate V against a viscous fluid flow possessing uniform velocity U distribution under specified supercooling ΔT (Fig. 8). The dendritic tip growth rate and radius, i.e., the main growth parameters of primary crystals, are obtained from the stationary model of axi-symmetric dendrite growth in a

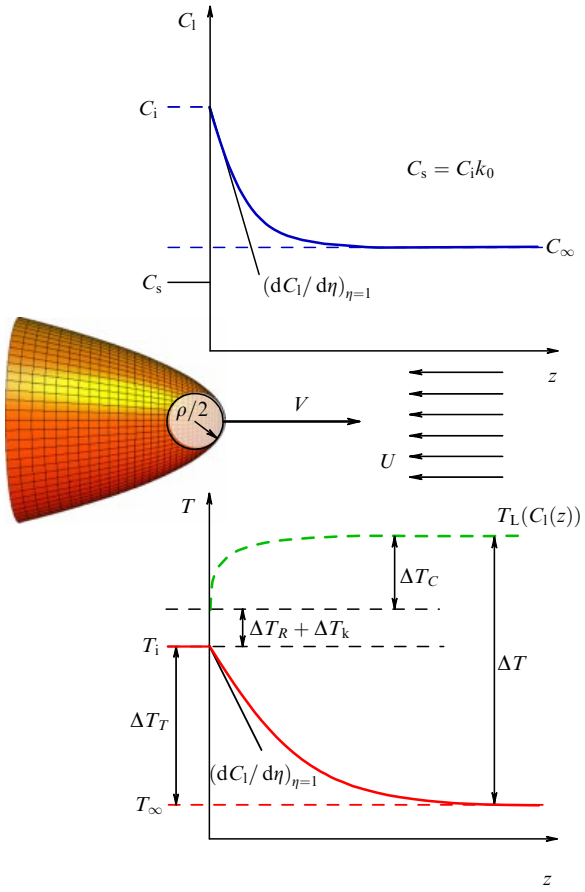

Figure 8. Concentration $C(z)$ and temperature $T(z)$ profiles in front of a paraboloidal dendrite tip. The tip with radius $\rho/2$ grows at a rate V against the counter flow of fluid having velocity U. Total supercooling $\Delta T = T_L - T_\infty$ is an experimentally measured quantity (T_L — liquidus temperature, T_∞ — temperature far from the dendrite tip), $dC_l/d\eta$ and $dT_l/d\eta$ are concentration and temperature gradients on the dendrite surface ($\eta = 1$) defined by expressions (10) and (11), respectively.

supercooled melt [9]. The expression for total supercooling $\Delta T = T_0 - mC_\infty - T_\infty$ is the first equation of the model and contains the contributions shown in Fig. 8. Here, C_∞ and T_∞ are the starting concentration and temperature, respectively, remaining constant far from the dendrite tip during its steady state growth. The balance equation at the dendritic tip (see Fig. 8) can be written out in the form

$$\Delta T = \Delta T_T + \Delta T_C + \Delta T_R + \Delta T_k\,. \tag{66}$$

Thermal supercooling ΔT_T in Eqn (66) is presented as

$$\Delta T_T \equiv T_i - T_\infty = \frac{Q}{c_p}\,\mathrm{Iv}\,(P_g, P_f)\,, \tag{67}$$

where the modified Ivantsov function $\mathrm{Iv}\,(P_g, P_f)$ defined by formula (16) has the form

$$\mathrm{Iv}\,(P_g, P_f) = P_g \exp\,(P_g + P_f)\, I_T(\infty)\,. \tag{68}$$

Integral I_T describes the conductive and convective mechanisms of heat transfer. It is defined by expression (13) for the growth of a parabolic plate in two-dimensional space, and by expression (59) for the growth of a paraboloid of revolution in three-dimensional space. The thermal Peclét numbers P_g and

P_f for the growing dendritic tip and convective fluid flow, respectively, are given by expressions [15].

The contribution ΔT_C to supercooling (66) from a temperature shift at the interface due to impurity is expressed as

$$\Delta T_C = m\,\frac{C_\infty(1-k_0)\,\mathrm{Iv}\,(P_{cg},P_{cf})}{1-(1-k_0)\,\mathrm{Iv}\,(P_{cg},P_{cf})}\,, \tag{69}$$

where the modified Ivantsov function assumes the form

$$\mathrm{Iv}\,(P_{cg},P_{cf}) = P_{cg}\exp\,(P_{cg}+P_{cf})\,I_C(\infty)\,. \tag{70}$$

Here, integral I_C is given by expression (14) for the parabolic plate growth in two-dimensional space, and by expression (60) for the growth of a paraboloid of revolution in three-dimensional space. The concentration (chemical) Peclét numbers take the form

$$P_{cg} = P_g\,\frac{D_T}{D_C} \equiv \frac{\rho V}{2D_C}\,,\quad P_{cf} = P_f\,\frac{D_T}{D_C} \equiv \frac{\rho U}{2D_C} \tag{71}$$

for the growing dendrite tip and the incoming convective fluid flow, respectively. Function $g(\eta)$ in expressions for viscous fluid flow is defined by formula (9) for the parabolic plate growth in two-dimensional space, and by formula (58) for the growth of a paraboloid of revolution in three-dimensional space.

The last contributions to balance (66) are found as follows. Contribution ΔT_R at the dendrite tip due to interface curvature (Gibbs–Thomson effect) is expressed as

$$\Delta T_R = \frac{2d_0Q}{c_p\rho}\,. \tag{72}$$

The contribution determining atomic kinetics intensity related to kinetic supercooling ΔT_k has the form

$$\Delta T_k = \frac{V}{\mu_k}\,, \tag{73}$$

where the kinetic coefficient μ_k characterizes the mechanism of atomic attachment to the interface.

Supercooling balance (66) is the first equation for determining two dendrite growth parameters: velocity V, and tip radius $\rho/2$. The second relation for determining V and ρ is selection condition (46) for the stable mode of steady-state dendritic tip growth in a viscous fluid:

$$\sigma^* \equiv \frac{2d_0D_T}{\rho^2V} = \sigma_0^*(\beta)\left[\frac{1}{2} - mC_i(1-k_0)\,\frac{D_Tc_p}{QD_C}\right]. \tag{74}$$

Here, C_i is the impurity concentration in the fluid at the dendrite tip (see Fig. 8):

$$C_i = \frac{C_\infty}{1-(1-k_0)\,\mathrm{Iv}\,(P_{cg},P_{cf})}\,, \tag{75}$$

and $\sigma_0^*(\beta)$ is the anisotropy parameter depending on $\beta = 15\varepsilon_c$, where ε_c is the interface anisotropy:

$$\sigma_0^*(\beta) = \frac{2\sigma_0\beta^{7/4}}{1+b\left(\beta^{-3/4}\alpha_0(\mathrm{Re})\right)^{11/14}}\,, \tag{76}$$

Table 1. Parameters of TiAl alloy (taken from Ref. [91]).

Parameter	Value
T_0 — solidification temperature, K	1748
C_∞ — impurity concentration, at.%	55
k_0 — distribution coefficient	0.8
m — liquidus slope, K (at.%)	8.8
D_C — diffusion coefficient in the liquid, $m^2\,s^{-1}$	8.27×10^{-9}
D_T — thermal diffusivity, $m^2\,s^{-1}$	7.5×10^{-6}
ν — kinematic viscosity of the liquid, $m^2\,s^{-1}$	0.5×10^{-7}
U — flow velocity, $m\,s^{-1}$	0.6
Q — latent heat of solidification, $J\,mol^{-1}$	12268.8
c_p — heat capacity, $J\,(mol\,K)^{-1}$	45
d_0 — capillary constant, m	7.8×10^{-10}
μ_k — kinetic coefficient at the interface, $m\,(s\,K)^{-1}$	0.209
ε_c — surface energy anisotropy	0.01
σ_0 — anisotropy constant	10.0
b — stability parameter	0.1

where σ_0 and b are numerical constants. The following expression holds for an incoming fluid flow:

$$\alpha_0(\mathrm{Re}) = \frac{d_0Ua(\mathrm{Re})\left[1+D_C/(2D_T)\right]}{4\rho V\left[D_C/(2D_T)+mC_i(1-k_0)\,c_p/Q\right]}\,, \tag{77}$$

including the parameter $a(\mathrm{Re})$ defined by equation (2) and formula (61) for the two-dimensional and three-dimensional cases, respectively.

6.2 Behavior of principal functions

In this section, we quantitatively characterize dendrite growth parameters and compare them with data obtained by numerical simulation applying the phase field method [90]. The parameters of the system used in the calculations are listed in Table 1.

6.2.1 Modified Ivantsov function. Figure 9 illustrates the solution of Eqn (68) taking account of functions (9), (13), and (15) for the modified Ivantsov function. It can be seen that the contribution from thermal supercooling, $\Delta T_T \propto \mathrm{Iv}(P_g,P_f)$, becomes smaller in the system with con-

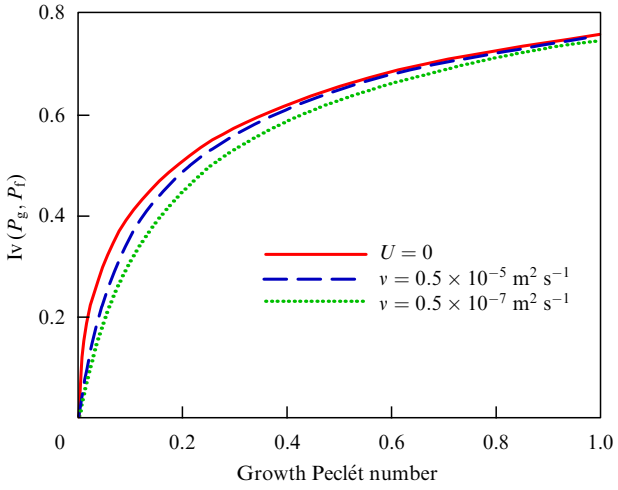

Figure 9. Modified Ivantsov function $\mathrm{Iv}\,(P_g,P_f)$ versus the growth Peclét number P_g under forced convection of the fluid with various kinematic viscosities ν. The curves are given for the values of the flow Peclét number $P_f = \nu\,\mathrm{Re}/(2D_T)$. Calculations for Iv were made for two-dimensional growth using Eqns (68) and taking account of functions (9), (13), and (15), as well as in comparison with the standard Ivantsov function $\mathrm{Iv}\,(P_g,P_f=0)$ for a stagnant fluid at $U=0$.

vective and conductive transport than in the one dominated by purely conductive heat transfer. The difference is due to the fact that the incident fluid flowing around the crystal enhances heat transfer and reduces the thermal contribution ΔT_T needed for a given dendritic tip growth rate V. A similar tendency emerges in the solution of the problem with an incoming ideal fluid [67]. The Ivantsov function at a fixed growth Peclét number decreases with decreasing viscosity (see Fig. 9), which suggests that the influence of convection on dendrite growth increases as the fluid viscosity decreases. Moreover, Fig. 9 confirms the earlier discussed significance of the convective heat transport effect [15, 17, 47] when the incoming fluid flow velocity is comparable to or lower than the dendrite tip growth rate.

Modified Ivantsov function (68) defines an infinite family of solutions relating supercooling ΔT to growth and flow Peclét numbers given by formulas (15). To estimate the influence of convection alone on the dendritic tip growth rate V and the tip radius $\rho/2$, the selection criteria (74)–(77) should be additionally used.

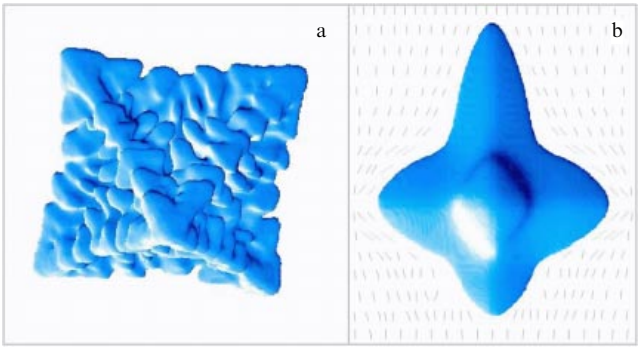

Figure 11. Results of modeling a dendritic crystal growing into a supercooled Ni melt. Calculations were done by the phase field method in three spatial dimensions [43]. (a) Dendritic structure without convective flow. Branching is due to stochastic noise in interface kinetics. (b) Dendritic structure growing in the convective counter flow with velocity 0.3 m s^{-1} directed from the top to bottom surfaces of the computational domain. No stochastic noise occurs at the interface.

6.2.2. Dendritic tip growth rate and radius. Solving the complete model (66)–(77) permits us to find the two main parameters: dendritic tip growth rate V, and dendrite tip radius $\rho/2$, whose stationary values determine the primary crystal structure. The present section reports the results of testing V and $\rho/2$ parameters found from the solution of the problem for a two-dimensional dendrite.

Figure 10 illustrate the action of an incoming melt flow on dendrite. The convective flow of fluid (solid curve) increases the dendritic tip growth rate over that in a stagnant melt (dashed curve). Generally speaking, the influence of the flow becomes most significant at small growth rates and supercoolings, when the flow velocity is comparable to or higher than the dendrite growth rate: $U \gtrsim V$. It follows from Fig. 10 that the tip growth rate at the flow velocity $U = 0.6$ m s^{-1} increases roughly tenfold (from 0.015 to 0.15 m s^{-1}) at a supercooling $\Delta T = 100$ K.

Notice that the results of calculations presented in Fig. 10 are directly related to the incoming flow shown in Fig. 8. The dendrite tip in the counter flow can be considered in the same manner as was done earlier using the phase field method [41, 42]. The influence of the flow on dendrite growth is illustrated in Fig. 11 by the results of modeling a dendritic crystal growing into a supercooled Ni melt. In a stagnant melt, the dendrite has geometrically identical branches (Fig. 11a), whereas the flow in the upper plane of the computational domain increases both the growth rate and the branch length oriented along the flow (Fig. 11b). The flow compresses the thermal interface layer in front of the protruding dendrite branch, thereby creating a greater temperature gradient and accelerating heat removal in comparison with those in the lower part of the dendrite. Indeed, an extended thermal layer forms around the downstream branch in the stagnant melt zone beneath the dendrite (at the bottom of the computational domain, Fig. 11b).

The estimated radius of a parabolic dendrite is shown in Fig. 12. It decreases under the effect of convection, thinning the dendrite. The qualitative result is that branches growing against the flow become thinner than those growing in a stagnant supercooled fluid. Therefore, 'thin' dendrites grow

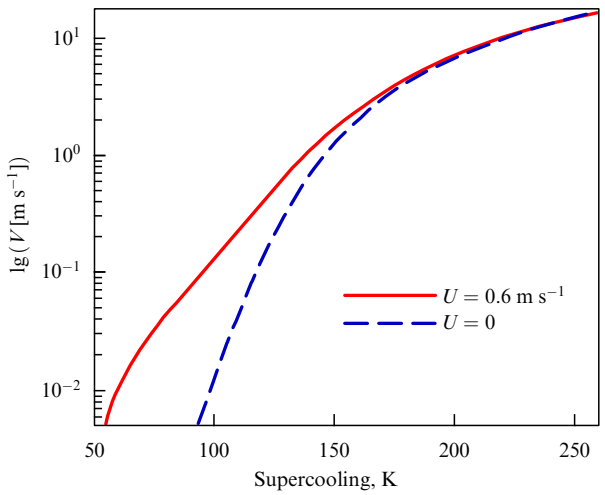

Figure 10. Logarithm of dendrite growth velocity, $\lg(V\,[\mathrm{m\,s^{-1}}])$, as a function of supercooling ΔT for the growth of a two-dimensional parabolic plate in a stagnant medium ($U = 0$) and in convective counter flow with velocity $U = 0.6$ m s^{-1}.

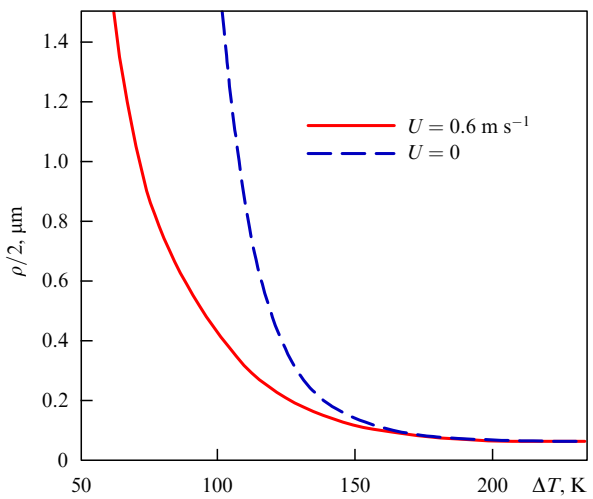

Figure 12. Dendrite tip radius $\rho/2$ of a growing parabolic two-dimensional plate as a function of supercooling ΔT in a stagnant medium ($U = 0$) and incident convective flow running with velocity $U = 0.6$ m s^{-1}.

faster than 'wide' ones over a supercooling range in which the flow velocity is comparable to the tip growth rate: $U \gtrsim V$. Figure 12 shows that the tip growth rate of a parabolic crystal increases from 3.8×10^{-7} to 1.3×10^{-6} m s^{-1}, i.e., by roughly an order of magnitude, at supercooling $\Delta T = 100$ K and fluid flow velocity $U = 0.6$ m s^{-1}. As follows from Figs 10 and 12, the counter flow at greater supercoolings, $\Delta T > 175$ K, has no effect on two growth parameters, V and ρ (given that the table parameters of the Ti–Al alloy are used). The flow affects the crystallization kinetics and crystal shape only in a range of growth rates comparable to the incoming flow velocity.

7. Comparison of theoretical predictions with experimental results

Conductive (molecular) and convective heat and mass transfer on a solidification front controls the crystal growth dynamics. Therefore, a reduction or complete suppression of convective transport under reduced gravity can markedly affect the crystalline microstructure of solidifible samples, permitting the use of experimental data on crystal growth kinetics to test theoretical models when estimating the effect of forced convection on microstructure formation under terrestrial and microgravity conditions [34, 44–46, 48, 49, 56, 67].

The Lorentz force arising in electromagnetic levitation lifts the sample, melts it, and induces mixing of melt (see Section 2). However, the Lorentz force arising under microgravity must be significantly smaller than in terrestrial experiments, which lowers the convection intensity in the droplets processed in an electromagnetic levitator. Both experiments and calculations [48] have demonstrated that dendrite growth in Ni–Al droplets slows down in EML under reduced gravity at supercoolings $\Delta T < 100$ K. Simultaneously, the crystalline structure becomes more homogeneous and contains fragmented grains. At a higher supercooling, $\Delta T > 100$ K, the dendrite growth rate in Ni–Al droplets is much higher than the convective flow velocity both under microgravity and terrestrial conditions. Therefore, the crystal growth rate measured from a recalescence front passage (see Refs [9, 17, 67] for the method) and the structure of solidified samples turn out to be similar in experiments of either type.

The qualitative verification of the theoretical model described in Section 6.1 is possible by comparing its results with crystallization kinetics data and the morphology of growing dendrites in a metal–metalloid Ni_2B system [67]. Ni_2B crystals are known to hold intermediate position among crystals grown by a conventional mechanism and having atomically rough facets and those grown by the tangential or stepwise mechanism and having atomically smooth facets. For this reason, modification of growth-controling parameters or ambient conditions in the case of Ni_2B crystals may give rise to structures with an atomically rough growth surface and macroscopically rounded dendritic branches or to structures with an atomically smooth growth surface and macroscopically faceted dendritic branches.

Figure 13 presents experimental data on the dendrite growth rate as a function of supercooling, obtained for droplets solidified in an electrostatic levitator (dark circles) and in an electromagnetic levitator (light squares) [92]. These experiments were designed to estimate the influence of forced convection on the growth rate and morphological changes in the Ni_2B crystal shape. Figure 13 shows that dendrite growth

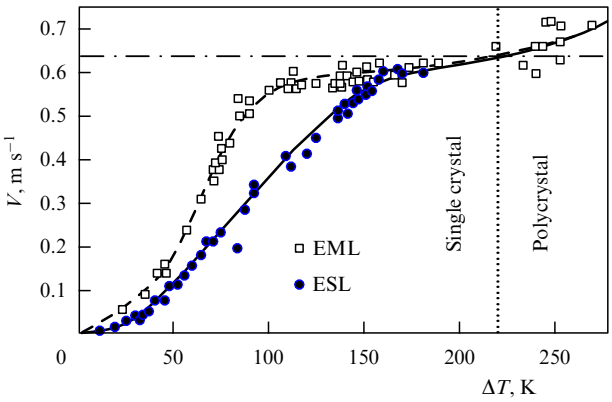

Figure 13. Experimental growth rates V of dendritic Ni_2B crystals, depending on initial supercooling ΔT (denoted by different symbols) [92]. Measurements were made for different intensities of forced convection: in an electrostatic levitator without convection ($U \approx 0$), and in an electromagnetic levitator in a convective flow with velocity $U \approx 0.25$ m s^{-1}. The curves correspond to calculations using equations (66)–(77).

rates measured in both ESLs and EMLs virtually coincide at both smallest and high supercoolings. This finding corresponds to the limiting cases of decreased influence of convection: (1) growth rates decrease, tending to zero (as $\Delta T \to 0$), and (2) dendrite growth rates are several times higher than the fluid velocity ($V \gg U$). However, the growth rates are significantly different in the intermediate supercooling range $30 \leqslant \Delta T \leqslant 180$ K. As was mentioned in Section 2, convective flow velocities in ESL-processed samples are much lower than in analogous droplet samples treated in EMLs, where flow velocities are comparable to the crystal growth rates. This accounts for the enhanced growth rates in EML samples when the principal direction of the liquid phase convective flow is opposite to the main direction of crystal growth.

Let us adopt the scheme of dendrite growth in a convective counter flow, shown in Figs 5 and 8. The basic equations (66)–(77) of the model, along with crystallographic and thermophysical parameters of the Ni_2B phase (see Ref. [92]), were utilized to calculate the dendritic growth rate as a function of supercooling. In addition to this set of equations, the peculiarities of the kinetic phase diagram were taken into account, determined by the liquidus slope and segregation coefficient in the functions of Ni_2B crystal growth rate [92, 93]. The results of calculations are shown in Fig. 13 by the solid curve for ESL experiments (in the absence of forced convection, $U = 0$) and the dashed curve for EML experiments. For the crystallization calculation of samples solidified in EML, the forced convection velocity was assumed to be $U \approx 0.25$ m s^{-1} (see papers [65, 67]). Figure 13 demonstrates that the model of dendrite growth under convection (see Section 6) adequately describes the experimental growth kinetics of the samples processed and crystallized in ESLs and EMLs. This result was achieved by introducing a forced convective flow into the model. For example, stability parameter (74) exerting a strong influence on the growth kinetics in the above supercooling range and the dendrite growth rate varies from $\sigma^* = 5.0 \times 10^{-5}$ in EML to $\sigma^* = 1.0 \times 10^{-4}$ in ESL, while the flow velocity falls from $U = 0.25$ m s^{-1} in EML to practically zero in ESL.

Convection affects not only the growth kinetics but also the growth form and even the crystal morphology of an Ni_2B

alloy. As shown in Ref. [92], droplike samples crystallized in ESL have a regular structure with macroscopically rounded dendrite tips, suggesting atomically rough growing facets. In contrast, Ni_2B alloy samples crystallized in EML have a single-crystalline facetted structure suggesting atomically smooth growing facets. Such an Ni_2B single crystal has a skeletal morphology (see Ref. [94]) analogous to the known morphology of bismuth crystals. The structure of an Ni_2B skeletal crystal is irregular and grows in a convective flow at a supercooling $\Delta T \lesssim 225$ K, i.e., in the ΔT region to the left of the dotted vertical line in Fig. 13. At higher supercoolings, $\Delta T \gtrsim 225$ K, when the influence of convection decays due to the high crystal growth rate, skeletal morphology, and facetted shape are succeeded by a dendritic polycrystal ensemble (in the ΔT region to the right of the dotted vertical line in Fig. 13).

Thus, it has been established that forced convection increases the growth rate of Ni_2B crystals, stabilizes the growth of atomically smooth facets, and changes the macroscopic growth form; specifically, the crystal habitus alters, i.e., a skeletal single crystal acquires a dendritic structure as its growth rate increases. Theoretical predictions based on calculations by the equations of model (66)–(77) quantitatively agree with experimental crystal growth rates with and without convection (see Fig. 13 and details of calculations in paper [92]). The applicability of the theory is confirmed by its agreement with experiment under terrestrial and reduced gravity conditions in EML and ESL facilities and with the use of the melt fluxing technique [93]. Further development of research and independent verification of the adequacy of the above models for the available experimental data on the changes of growing crystal morphology should be focused on numerical simulations of solidification, taking account of the anisotropic properties of moving liquid–crystal interfaces and convective flows.

8. Conclusion

The theory considered in this review and the relevant experimental data provide a basis for the formulation of an approach to the problem of dendritic crystal growth under liquid phase convection. The analytical solution to the problem of the selection of the stable dendritic tip growth regime in a binary system under forced convective flow of fluid is proposed.

An analysis of the stable regime yields the criterion for dendritic tip growth in a binary system, taking into consideration convection and the anisotropy of surface tension at the crystal–melt interface. The stable growth criterion can be extended to the arbitrary Peclét numbers P_g [87] and to the description of dendritic crystal growth on the surface of Earth's solid core adjoining the liquid one [89].

The review presents, with reference to the dendritic tip growth criterion, the model for qualitative analysis and quantitative computation of the influence of a fluid flow on the parameters of dendrite growth [see expressions (66)–(77)]. The model describes crystal growth in a viscous and weakly viscous liquids, which makes it applicable to real melts and solutions. In particular, it shows that the influence of convection on the dendrite growth rate increases with decreasing viscosity over a wide supercooling range (see Fig. 9).

The model of dendritic crystal growth includes the following limiting cases:

— equations for dendrite growth in an ideal liquid, i.e., at zero viscosity, $v \to 0$ (corresponding to the solutions from Ref. [31]);

— equations for dendrite growth in a one-component supercooled system in the absence of the second component concentration, i.e., at $C_\infty = 0$ (corresponding to the solutions from Ref. [32]);

— equations for dendrite growth in a stagnant binary system, i.e., at $U = 0$ (corresponding to the solutions from Ref. [33]).

The special limiting case of the model concerns the calculation of the 'concentration' dendrite (i.e., 'chemical' or 'solutal' crystal) growing in a binary, i.e., composed of two chemical components, system at constant temperature. The theory in question is generalized to criterion (65) determining the stable growth of dendritic tips in a chemically multicomponent system under convection at an arbitrary growth Peclét number and anisotropic surface tension at the interface.

The review leads us to recognize that the theory of dendrite growth under forced convection can be applied to

— verify the results of numerical simulations of dendrite growth;

— interpret experimental data on crystal growth under microgravity (when convective flow is very slow) and Earth's (when the role of convection in crystal growth kinetics markedly increases) conditions.

Indeed, it is shown by an example of crystal growth from an Ni_2B melt that the above approach makes it possible to predict the results of crystallization kinetics experiments and the morphological features of crystal structure, depending on convective flow intensity.

Acknowledgments

The authors are grateful to Dieter Herlach for the long-term cooperation in experimental and theoretical research on new materials, and S Binder, M Kolbe, H Möller, S Reutzel, Th Volkmann, and D Holland-Moritz for experimental verification of the theory and fruitful discussions of its results. We also thank V S Yuferev for reading the manuscript and the helpful criticism. The work was partly supported by the Laboratory of Multiscale Mathematical Modeling, Ural Federal University, Deutscher Akademischer Austauschdienst (DAAD), the Russian Federation Ministry of Education and Science (project No. 11.9139.2014), the Russian Research Fund, the European Space Agency (project MULTIPHAS, ESA-ELIPS AO-2004-144), and Deutsches Zentrum für Luft- und Raumfahrt (contract 50WM1140).

References

1. Chernov A A, in *Modern Crystallography III*: *Crystal Growth* (Ed.-in-Chief B K Vainshtein) (Berlin: Springer-Verlag, 1984); Translated from Russian: in *Sovremennaya Kristallografiya* Vol. 3 (Ed.-in-Chief B K Vainshtein) (Moscow: Nauka, 1980) p. 3
2. Borisov V T *Teoriya Dvukhfaznoi Zony Metallicheskogo Slitka* (The Theory of Two-phase Zone in a Metal Ingot) (Moscow: Metallurgiya, 1987)
3. Trivedi R, Kurz W *Int. Mater. Rev.* **39** 49 (1994)
4. Ovsienko D E *Zarozhdenie i Rost Kristallov iz Rasplava* (Crystal Nucleation and Growth from Melts) (Kiev: Naukova Dumka, 1994)
5. Galenko P K, Zhuravlev V A *Physics of Dendrites* (Singapore: World Scientific, 1994)
6. Fedorov O P *Protsessy Rosta Kristallov*: *Kinetika, Formoobrazovanie, Neodnorodnosti* (Crystal Growth Processes: Kinetics, Formation, Inhomogeneities) (Kiev: Naukova Dumka, 2010)

7. Kurz W, Fisher D J *Fundamentals of Solidification* 3rd ed. (Aedermannsdorf: Trans Tech Publ., 1989)
8. Zhuravlev V A *Zatverdevanie i Kristallizatsiya Splavov s Geteroperekhodami* (Solidification and Crystallization of Heterotransition Alloys) (Moscow: Inst. Komp'yut. Issled., RKhD, 2006)
9. Herlach D, Galenko P, Holland-Moritz D *Metastable Solids from Undercooled Melts* (Amsterdam: Elsevier, 2007)
10. Herlach D M, Galenko P K, Hartmann H *Rubin Wissenschaftsmag. Ruhr Univ. Bochum* (3 – 5) 30 (2008)
11. Langer J S *Rev. Mod. Phys.* **52** 1 (1980)
12. Umantsev A R, Vinogradov V V, Borisov V T *Sov. Phys. Crystallogr.* **31** 596 (1986); *Kristallografiya* **31** 1002 (1986)
13. Boettinger W J et al. *Annu. Rev. Mater. Res.* **32** 163 (2002)
14. Asta M et al. *Acta Mater.* **57** 941 (2009)
15. Eckler K, Herlach D M *Mater. Sci. Eng. A* **178** 159 (1994)
16. Galenko P K et al. *Mater. Sci. Eng. A* **375 – 377** 488 (2004)
17. Funke O et al. *J. Cryst. Growth* **297** 211 (2006)
18. Ivantsov G P *Dokl. Akad. Nauk SSSR* **58** 567 (1947)
19. Ivantsov G P *Dokl. Akad. Nauk SSSR* **83** 573 (1952)
20. Ivantsov G P, in *Rost Kristallov. Materialy Vtorogo Soveshchaniya po Rostu Kristallov, Moskva, 23 Marta – 1 Aprelya 1959 g* (Proc. of the Second Meeting on Crystal Growth, Moscow, March 23 – April 1, 1959) Vol. 3 (Exec. Eds A V Shubnikov, N N Sheftal') (Moscow: Izd. AN SSSR, 1961)
21. Temkin D E *Dokl. Akad. Nauk SSSR* **132** 1307 (1960)
22. Temkin D E *Kristallografiya* **7** 446 (1962)
23. Horvay G, Cahn J W *Acta Metallurg.* **9** 695 (1961)
24. Mullins W W, Sekerka R F *J. Appl. Phys.* **35** 444 (1964)
25. Nash G E, Glicksman M E *Acta Metallurg.* **22** 1283 (1974)
26. Langer J S, Müller-Krumbhaar H *Acta Metallurg.* **26** 1681 (1978)
27. Willnecker R, Herlach D M, Feuerbacher B *Phys. Rev. Lett.* **62** 2707 (1989)
28. Kessler D A, Koplik J, Levine H *Adv. Phys.* **37** 255 (1988)
29. Brener E, Melnikov V I *Adv. Phys.* **40** 53 (1991)
30. Dash S K, Gill W N *Int. J. Heat Mass Trans.* **27** 1345 (1984)
31. Benamar M, Bouissou Ph, Pelce P *J. Cryst. Growth* **92** 97 (1988)
32. Bouissou Ph, Pelcé P *Phys. Rev. A* **40** 6673 (1989)
33. Ben Amar M, Pelcé P *Phys. Rev. A* **39** 4263 (1989)
34. Galenko P K, Herlach D M, in *Phase Transformations in Multicomponent Melts* (Ed. D M Herlach) (Weinheim: Wiley-VCH, 2008) p. 353
35. Herlach D M *Annu. Rev. Mater. Sci.* **21** 23 (1991)
36. Herlach D M et al. *Int. Mater. Rev.* **38** 273 (1993)
37. Herlach D M *Mater. Sci. Eng. R* **12** 177 (1994)
38. Glicksman M E, Koss M B, Winsa E A *Phys. Rev. Lett.* **73** 573 (1994)
39. Mathiesen R H et al. *Metallurg. Mater. Trans. A* **37** 2515 (2006)
40. Ruvalcaba D et al. *Acta Mater.* **55** 4287 (2007)
41. Ramirez J C, Beckermann C *Acta Mater.* **53** 1721 (2005)
42. Jeong J-H, Goldenfeld N, Dantzig J A *Phys. Rev. E* **64** 041602 (2001)
43. Galenko P K et al., in *Computational Modeling and Simulation of Materials III. Proc. of the 3rd Intern. Conf., Acireale, Sicily, Italy, May 30 – June 4, 2004* Pt. B (Eds P Vincenzini, A Lami, F Zerbetto) (Faenza: Techna, 2004) p. 565
44. Hyers R W et al. *Ann. New York Acad. Sci.* **1027** 474 (2004)
45. Volkmann Th et al., in *Phase Transformations in Multicomponent Melts* (Ed. D M Herlach) (Weinheim: Wiley-VCH, 2008) p. 227
46. Matson D M et al. *J. Jpn. Soc. Microgr. Appl.* **27** 238 (2010)
47. Herlach D M, Galenko P K *Mater. Sci. Eng. A* **449 – 451** 34 (2007)
48. Reutzel S et al. *Appl. Phys. Lett.* **91** 041913 (2007)
49. Reutzel S et al., in *Proc. of the 59th Intern. Astronautical Congress, IAC 2008, Glasgow, Scotland, 29 September – 3 October 2008* Vol. 1 (Red Hook, NY: Curran Associates, Inc., 2008) p. 593
50. Schwarz M et al. *Phys. Rev. Lett.* **73** 1380 (1994)
51. Karma A *Int. J. Non-Equilibrium Processes* **11** 201 (1998)
52. Lipton J, Glicksman M E, Kurz W *Metallurg. Trans. A* **18** 341 (1987)
53. Lipton J, Kurz W, Trivedi R *Acta Metallurg.* **35** 957 (1987)
54. Alexandrov D V, Galenko P K, Herlach D M *J. Cryst. Growth* **312** 2122 (2010)
55. Alexandrov D V, Malygin A P, Galenko P K, in *Proc. 8th Intern. Conf. on Heat Transfer, Fluid Mechanics and Thermodynamics, Mauritius, 11 – 13 July 2011*, p. 299
56. Herlach D M, Galenko P K *J. Jpn. Soc. Microgr. Appl.* **27** 245 (2010)
57. Davidoff E et al. *Acta Mater.* **61** 1078 (2013)
58. Chan S-K, Reimer H H, Kahlweit M *J. Cryst. Growth* **32** 303 (1976)
59. Huang S-C, Glicksman M E *Acta Metallurg.* **29** 701 (1981)
60. Emsellem V, Tabeling P *J. Cryst. Growth* **156** 285 (1995)
61. Herlach D M, Matson D M (Eds) *Solidification of Containerless Undercooled Melts* (Weinheim: Wiley-VCH, 2012)
62. Meister T et al. *Control Eng. Practice* **11** (2) 117 (2003)
63. Flemings M C et al. "Levitation observation of dendrite evolution in steel ternary alloy rapid solidification (LODESTARS)", NASA Science Requirement Document LODESTARS-RQMT-0001 (Washington, DC: NASA, 2003)
64. Matson D M, Hyers R W, Volkmann Th *J. Jpn. Soc. Microgr. Appl.* **27** (4) 238 (2010)
65. Hyers R W, in *Solidification of Containerless Undercooled Melts* (Eds D M Herlach, D M Matson) (Weinheim: Wiley-VCH, 2012) p. 31
66. Tourret D et al. *Acta Mater.* **59** 4665 (2011)
67. Binder S, PhD Thesis (Bochum: Ruhr Univ., 2010)
68. Bojarevich V, Kao A, Pericleous K, in *Solidification of Containerless Undercooled Melts* (Eds D M Herlach, D M Matson) (Weinheim: Wiley-VCH, 2012) p. 321
69. Meirmanov A M *The Stefan Problem* (Berlin: Walter de Gruyter, 1992)
70. Gupta S C *Classical Stefan Problem* (Amsterdam: Elsevier, 2003)
71. Lamb H (Sir) *Hydrodynamics* (New York: Dover Publ., 1945); Translated into Russian: *Gidrodinamika* (Moscow–Leningrad: Gostekhizdat, 1947)
72. Kochin N E, Kibel', I A, Roze N V *Theoretical Hydromechanics* (New York: Interscience Publ., 1964); Translated from Russian: *Teoreticheskaya Gidromekhanika* Pt. 2 (Leningrad–Moscow: Gostekhizdat, 1948)
73. Kessler D A, Koplik J, Levine H *Phys. Rev. A* **33** 3352 (1986)
74. Barbieri A, Langer J S *Phys. Rev. A* **39** 5314 (1989)
75. Pelcé P, Bensimon D *Nucl. Phys. B Proc. Suppl.* **2** 259 (1987)
76. Pelcé P (Ed.) *Dynamics of Curved Fronts* (Boston: Academic Press, 1988)
77. Fröman N, Fröman P O *JWKB Approximation*: *Contributions to the Theory* (Amsterdam: North-Holland, 1965); Translated into Russian: *VKB-Priblizhenie* (Moscow: Mir, 1967)
78. Zel'dovich Ya B et al. *Combust. Sci. Technol.* **24** 1 (1980)
79. Caroli B et al. *Phys. Rev. A* **33** 442 (1986)
80. Galenko P et al. *Acta Mater.* **55** 6834 (2007)
81. Galenko P et al. *Acta Mater.* **57** 6166 (2009)
82. Bouissou P, Perrin B, Tabeling P *Phys. Rev. A* **40** 509(R) (1989)
83. Kurnatowski M, Grillenbeck Th, Kassner K *Phys. Rev. E* **87** 042405 (2013)
84. Tong X et al. *Phys. Rev. E* **63** 061601 (2001)
85. Trivedi R, Kurz W *Acta Metallurg.* **34** 1663 (1986)
86. Galenko P K, Danilov D A *Phys. Rev. E* **69** 051608 (2004)
87. Alexandrov D V, Galenko P K *Phys. Rev. E* **87** 062403 (2013)
88. Alexandrov D V, Pinigin D A *Tech. Phys.* **58** 309 (2013); *Zh. Tekh. Fiz.* **83** (3) 1 (2013)
89. Alexandrov D V, Galenko P K *J. Phys. A Math. Theor.* **46** 195101 (2013)
90. Galenko P K, Binder S, Ehlen G J, in *Solidification of Containerless Undercooled Melts* (Eds D M Herlach, D M Matson) (Weinheim: Wiley-VCH, 2012) p. 349
91. Hartmann H et al. *J. Appl. Phys.* **103** 073509 (2008)
92. Binder S, Galenko P K, Herlach D M *Phil. Mag. Lett.* **93** 608 (2013)
93. Binder S, Galenko P K, Herlach D M *J. Appl. Phys.* **115** 053511 (2014)
94. Shubnikov A V, Parvov V F *Zarozhdenie i Rost Kristallov* (Crystal Nucleation and Growth) (Moscow: Nauka, 1969)